FOCUSED LASER SPIKE DEWETTING AS A METHOD TO PROBE RHEOLOGY OF POLYMER THIN FILMS

By

ADITHYA SRIDHAR

A thesis submitted to the

School of Graduate Studies

Rutgers, The State University of New Jersey

In partial fulfillment of the requirements

For the degree of

Master of Science

Graduate Program in Mechanical and Aerospace Engineering

Written under the direction of

Jonathan P. Singer

And approved by

_____

_____

_____

New Brunswick, New Jersey

October, 2018

ABSTRACT OF THE THESIS

FOCUSED LASER SPIKE DEWETTING AS A METHOD TO PROBE RHEOLOGY OF POLYMER THIN FILMS

By ADITHYA SRIDHAR

Thesis Director:

Jonathan P. Singer

Thin polymer films whose thickness ranges from fractions of a nanometer to several micrometers have been in high demand over the past few years in several industries. Their high surface area to volume ratio and the potential for low-cost processing with minimal material usage while fulfilling purpose requirements make them very useful. However, these films behave differently from bulk materials and majority of polymer fabrication processes involve polymer flow. Hence the study of polymer thin film rheology becomes crucial. Bulk measurement of rheology is well established, but it has disadvantages in that it requires a lot of material and may not capture thin film physics. Previous studies have demonstrated dewetting of thin polymer films to study film material stability and properties. This study seeks to use focused laser spike (FLaSk) dewetting as a method to probe rheology of thin material films. The method is used to extract materials properties of three thin films – Polystyrene (PS), Poly –4–hydroxystyrene (PHS) and N, N′-Bis (3 – methylphenyl)–N, N′-diphenylbenzidine (TPD) having different glass transition temperatures, T_g, and molecular weights, MW. The three thin films are placed on a heating substrate which is subjected to FLaSk dewetting process for a range of laser powers and

exposure times. The intensity of the metal fluorescence of the substrate, which is assumed to be a function of the local temperature, is analyzed. The dewetted spots are then analyzed using an optical microscope and characterized by the several characteristic radii. The obtained radii values are then studied with respect to laser power and intensity, where early stage evolution and dewetting is observed. The growth of the radii is then studied as a function of exposure time and laser spot intensity. The trends indicated the expected involvement of surface behavior along with bulk behavior, and we are able to observe materials-consistent thermally-dependent behavior. By incorporating the ability to physically measure the local instantaneous temperature and conducting more experiments with well-studied materials would propel the next step in realizing the potential of FLaSk dewetting being a method to probe material film properties.

ACKNOWLEDGEMENT

This study is a result of a year of arduous work which would have not been possible without a lot of people. I would like to take this opportunity to express my profound gratitude to my thesis advisor, Professor Jonathan P. Singer for his patient guidance enthusiastic encouragement and useful critique of this research work. First and for most I would like to thank him for giving me the privilege to work on a topic that is practical, interesting, and has scope for further study and implementation. I also had the privilege of taking Professor Singers Thermodynamic Theory course. The large number of thought provoking and invigorating questions put forth by him during various stages of the course and the research work required me to read and understand deep into the subject matter which expanded my knowledge. On multiple occasions he shared his invaluable experience to help improve my clarity in thinking. I would also like to thank the entire HMNL lab team and Mr. John Petrowski for making all the resources required to complete this work available at all times. I would like to express my gratitude to Tianxing Ma for taking valuable time out of his doctorate dissertation work to help me understand the process, taking time out to teach me and help me get to grips with the lab instruments and most importantly making himself available when required. I would also like to thank Matthew Signorelli for helping develop a program to identify the dewet spot center. I would like to thank the committee members for taking valuable time out of their busy schedule to peruse this thesis and also participate in the defense. Finally, I would like to thank my friends and my family-Sridhar and Narayanan for their constant support and encouragement which has made this entire endeavor possible.

TABLE OF CONTENTS

LIST OF ILLUSTRATIONS

CHAPTER 1 – LITERATURE SURVEY

1.1 Thin Films

The demand for small device development has seen an upsurge in the past decades and will continue to see an upsurge in the future. Fundamental to these devices are thin films. These films are omnipresent and they are utilized in multiple purposes ranging all the way from item packaging to the manufacturing of integrated circuits. Thin film as the name implies is a layer of material whose thickness ranges from fractions of a nanometer to several micrometers, usually deposited on a metal, ceramic or semiconductor substrate. Thin films have a high surface area to volume ratio and this allows them to be treated as a two-dimensional system, which is of great importance and helps solve many real-world problems. The importance of these films is realized from the fact that they possess the potential for low-cost processing with minimal material usage while fulfilling purpose requirements. As a result, this helps enable cost-effective applications for raw source materials that can prove to be expensive. Thin films of a particular chemical composition behave differently from bulk materials of the same chemical composition in several ways. For instance, thin films are sensitive to surface properties while bulk materials typically are not. Thin films are also relatively more sensitive to thermomechanical stresses and can enable applications where low weight and high mechanical flexibility are a priority. When compared to bulk materials, thin film made of the same material costs much less, yet they perform the same function when it comes to surface processes. As mentioned earlier, thin films are used across various fields such as microelectronics,

communication, optical electronics, catalysis, coating of all kinds and many more. Thin films are being used in microelectronics industry, where they are being used as photoresist layers [1]. Recently they have been found to be an emerging platform for drug delivery [2]**.** Their thin and flexible nature has led them to be perceived to be less obtrusive and more acceptable by the patient as opposed to traditional drug delivery methods. Their ability to prevent metal corrosion has seen them being utilized as physical and chemical coatings [1]**.** Thin films have also found increased use in another field of medicine – dentistry. This increasing interest is attributed due to the excellent surfaces properties of thin films and their mechanical properties, low production cost, and ease in processing, allowing them to be tailored for a wide range of applications such as reducing friction, preventing bacterial biofilm and restorative dentistry among others [3]. Thin films have also found opportunities for applications in sensing technologies [4]. Previously sensors could not be used in conjunction with soft contact lenses due to the curved nature of a lens. However, with the properties exhibited by thin films, studies are currently carried out by integrating thin film sensors with commercially available soft contact lenses [5]. These thin film sensors embedded on the soft contact lens have the ability to detect glucose, lactate and pH levels providing information associated with eye health and results in numerous advanced eye care applications. With an already wide range of thin film applications existing, in order to develop new technologies for future applications, it is highly essential to obtain knowledge and determination of the nature, functions and new properties of thin films. These novel innovations come with inherent challenges. For instance, in the case of a thin film soft contact sensor lens, the layer must uniformly cover the eye surface and it has to stay stable during the blinking time of the eye. The film must not break or dewet under any

circumstance. Therefore, it is critical to establish an understanding of the physical, chemical and rheological properties which influence the stability of a thin film. In such cases and many more, it has become essential to understand the rheological properties of thin films and the role played by interactions at the solid – liquid interface of thin films, and this has been the subject of extensive research in the material science field in the previous years.

1.2 Polymers

In day-to-day life polymers play an omnipresent role. They serve a wide array of purposes ranging all the way from common plastics such as item packaging to specialized polymer materials in electronics, healthcare and military components. Polymers generally possess a high molecular weight, MW which is achieved by linking together molecules into a chain-like structure. This quest for unending research in polymer science and demand for polymers is that they are extremely flexible among all materials and their mechanical properties range all the way from flexible gels and rubbers to string fibers. This stems from the design of the repeating molecule structure and control of the entire chain length and structure [6]. As a result, most of the research is focused on analyzing the chain structure and develop a universal model. This universal model researchers hope would ideally encapsulate all the polymer behavior in terms of the chain characteristics-length, width and interactions with neighboring chains. Rheological behavior is one field where extensive research has been conducted by working on models for the chain motions and extensive characterization of a large numbers of polymer structures. The reason behind increasing interest in rheology is closely associated with the physical and chemical behavior of important polymers. In the case of commercial use of polymers, both the mechanical

properties of the polymer and the ability to fabricate the polymer take importance. For instance, with linear polymer chains, a longer chain structure is desired as it results in a higher MW which in turn results in desired mechanical properties. However, an increase in chain length results in viscosity increase which may be detrimental to the necessary fabrication process. For instance, polythene a commonly used polymer at a MW of 100000 g / mol has reasonable properties and is easy to process. Polythene at mid – to – high MW range has improved strength but processing difficulty increases. However, polyethene at extreme high MW range results in the best properties but is extremely difficult to process. Therefore, if the polymer cannot be fabricated quickly and inexpensively then the polymers properties become irrelevant, no matter how desirable they turn out to be. The majority of polymer processing and fabrication processes involve polymer flow and this is where study of polymer rheology becomes crucial.

1.3 Glass Transition Temperature

Molecules possess the ability to exist in three possible physical states – solid, liquid, and gas. Polymers do not possess such a straightforward classification. For instance, in the case of many polymers, the transition between solid and liquid states in polymers is very difficult to pinpoint. Structurally however, polymers can be classified as amorphous or crystalline in the solid state. In the amorphous state the arrangement of the polymer molecules is a random arrangement and the polymer does not have a well-defined structure and repeating arrangement of polymer chains. In the crystalline state the polymer molecules have a well-defined structured and a repeating arrangement of polymer chains. The normal state of polymers at room temperature is an amorphous state. At temperatures below the glass transition temperature T_g, the polymer molecular chains do not contain

enough energy to allow them to drift or move. This ensures that the molecules are essentially locked into a rigid amorphous structure. However, when heat is applied, the molecules gain energy and they have the ability to move. If heat is still applied, at some point the energy obtained is enough to bring about a change in the state. The polymer structure changes from an amorphous rigid structure to a flexible structure. The polymer molecules move freely around each other. This transition temperature is called the glass transition temperature. T_g of a polymer system defines the change in state of a polymer from a rigid amorphous state to a flexible state. The T_g results in a change in the polymer heat capacity. The polymer does not melt, it simply undergoes a change in structure-from being amorphous to a flexible state. This produces a change in the heat capacity of the material. T_g applies only to polymers in amorphous state. A polymer in the crystalline state will melt when heat is applied. The T_g of glassy thin films are extremely sensitive to the nature of the surface. Polystyrene thin films are studied the most in this regard [7-10]. T_g can be used to estimate performance parameters of polymers [11]. Physical mixtures of multiple polymers also known as polymer blends can be either uniform or non-compatible. In non-compatible blends each component exhibits clear T_g and in uniform blends there is a single T_g. Therefore, analysis and knowledge of these temperatures provide data regarding polymer compatibility. In the T_g region, quantity of residual strains can be measured by conduction torsion tests on the polymer solid sample.

1.4 Rheology

Deriving its definition from the Greek work Rheos (ρει) which stands for flow, Rheology is defined as the science of deformation and flow of materials. In simpler terms, rheology is a study related to how the stress in a material is related to deformation of the material.

In the case of simple fluids, rheology study involves viscosity measurement. However, in the case of polymers, their flow depicts nonideal behavior and as result rheology study is more complicated. Polymer flow shows complex shear viscosity behavior, elastic properties, normal stress phenomena and prominent tensile viscosity. The above polymer rheological properties depend on the shear rate, the MW, polymer structure and the temperature. The goal behind conducting rheology studies is to understand the types of flow and deformation effects exhibited by polymer flow. The flow and deformation knowledge can then be used to apply qualitative rheological knowledge and quantitative analytical ideas and means to analyze rheological effects.

1.4.1 Rheology Measurement

Rheometer measurements generally involve measuring two quantities – stress, which is defined as the amount of force applied per unit area on the material; and strain, which is defined as the degree to which the material deforms. Material properties which can be quantified as elastic moduli for solids is calculated using the ratio of stress to strain, or viscosity for liquids can be calculated using the ratio of stress to strain rate. Experimental rheology is concerned with the development of new methods, techniques and instruments to measure the rheological parameters, such as the shear viscosity η_s, the storage modulus G' and loss modulus G''. Computational rheology deals involve constructing and using equations, which are able to predict the rheological properties. However, complex soft materials depict viscoelastic properties and hence the relation of stress to strain must be measured over a wide range of strains, strain rates, and time scales [12]. Polymers are used in industrial processing in operations, such as extrusion, wire coating, thermoforming. The design and analysis for such operations is complicated because of the processes and the

interaction of material – polymer melt and machine. Studies have been conducted in the computational rheology field where new and complex models have been developed to deal with the viscoelasticity of the polymer melts [13]. The study demonstrates that simulation of polymer processes offers a unique challenge and accurate computational rheological models will help in the analysis and development of polymer processing method. Advances have been made in developing new rheological methods to measure materials with complex time-dependent responses at the micron scale. Soft materials respond differently under large strains and this makes them extremely purposeful. A good example of soft materials would be biological tissues such as lungs and blood vessels that stretch and expand under normal use, but stretch even more during injury. Soft tissues stiffen with increasing strain and thereby demonstrate nonlinear viscoelastic response. This is termed as strain stiffening. Studies have shown that biopolymers such as collagen demonstrate nonlinear elasticity at strains where cross-linked flexible polymers like elastomers demonstrate a linear elastic response [14] [15]. Polyacrylamide, a flexible polymer gel is an example of this comparison where nonlinear responses of semiflexible polymers present difficult challenges for using experimental methods or developing new theories. A few approaches have been developed to analyze strain-stiffening soft materials. It has been studied that if the material exhibits very little creep, a constant stress can be imposed to produce a given amount of strain, and then a small incremental oscillatory stress is superimposed which results in a nearly sinusoidal strain response [16]. Studies showed that the incremental measurement reflects the stiffness of the sample in the deformed state [17]. The other approach involved plotting the instantaneous stress and strain data from each oscillation on orthogonal axes, using a method termed large amplitude oscillatory shear analysis [18].

The storage and loss moduli are then be calculated from the ascending and descending part of the sinusoid, slopes and differences between the stress at a particular strain. In many cases, macroscopic response of a material which arises because of material deformation cannot be simply characterized by non-linear measurements, such as measurement of stress or strain alone. Soft materials sheared at large amplitudes can undergo structural transitions such as crystallization or shear banding, and these transitions confuse analysis and interpretation unless there exists a model that anticipates their existence. Studies have showed that in shear banding the sheared material separates into regions characterized by different viscosities [19] [20]. Therefore, the same measured stress value can result from multiple strain rates. Rheo-optical characterization depends on whether the information is obtained by real-space imaging or by scattering in reciprocal space. Studies have been conducted to study this structural characterization. Real-space techniques involve the use of fluorescence microscopy or magnetic resonance imaging [21] to image through a rheometer. Scattering techniques utilize X-rays measuring changes in scattering patterns using light. Studies are also conducted where rheology of complex fluids where studied using dynamic light scattering. Dynamic light scattering was used to measure linear viscoelasticity moduli of complex fluids, which was dependent on frequency [22]. This was achieved by comparing the relaxation of thermal excitations of a probe particle to the viscoelastic properties of the surrounding medium, also known as the fluctuation dissipation theorem. The advantage with this method was that the linear viscoelastic moduli could be probed over a much larger frequency range than traditional mechanical means, thereby extending their measurement to higher frequencies. Rheology studies have also been conducted to provide a more complete characterization of the structure and properties

of new nanocomposite materials [23]. The melt-state linear and nonlinear shear rheological properties of hybrid materials of polypropylene were studied. The study showed that transient nonlinear rheology is consistent with an anisometric and non-Brownian structure. It was shown that rheological methods probe hybrid structures only indirectly; however, using rheology probing in conjunction with standard methods such as electron microscopy, and mechanical testing indicated the potential usefulness of such studies for the development of new nanocomposite materials. Studies conducted on thin polymer films have demonstrated that physical properties of thin films exhibited characteristics largely deviating from bulk behavior of the same polymer material. Studies have shown density changes occurring if the thin film is annealed below the polymer bulk T_g. Instabilities in thin films have been unexpected as demonstrated by studies [24]. T_g has shown to be thickness-dependent and also polymer film history-dependent [25]. Rheological measurement of polymers in their bulk state is achieved with less complications. Measuring macroscopic properties of viscoelastic polymers involve dynamic testing such as alternating current (AC) modulation techniques, which give the properties of a material as a function of frequency. This allows the time-dependence of the mechanical behavior of a viscoelastic material to be measured. Rheological measurements of polymers in bulk state require films to have a thickness of at least 0.5 mm and a diameter of at least 4 mm. Complications arise when the state size is reduced, such as thin films and cells. In such cases, flow properties are difficult to analyze, measure and understand. Certain studies conducted have demonstrated the ability to probe the rheological properties of polymer films that have thickness ~10 nanometers by taking advantage of surface tension properties [26]. The study involved preparing of stepped bilayer films of the same polymer on a

substrate. The film when annealed above the T_g results in broadening of the film height profiles. The rate at which the broadening takes place was controlled by varying the MW of the films. The method was then used to measure viscosity differences of a polymer melt with a change in MW, thus establishing the stepped film geometry as a method to the measure rheological properties in thin films. Thin film confinement can alter properties from the corresponding polymer bulk material property, such as T_g as demonstrated by certain studies [27]. Probing rheology of thin polystyrene films was studied by investigating growth dynamics of wetting ridges. Wetting ridges–a ridge like deformation can be formed by depositing a non–movable droplet whose volume is in the nanoliter to microliter range, also called a sessile droplet on a polymer surface. This is formed under the traction of the liquid surface tension. The study showed that rheology of thin polystyrene films can be studied using the growth of the wetting ridge [28]. The study showed that investigating change in wetting ridge height with polymer film temperature, the temperature spectrum of thin polymer film mechanical properties could be obtained and the viscoelastic behavior of thin polymer films can be studied. Rheological properties of the polymer thin film such as T_g can consequently be extracted from the height–temperature curves. Thereby, growth of the wetting ridge provides a potential method for determining the viscoelastic properties of thin polymer films under the condition that the film does not dewet. However, study conducted for the thin polystyrene film on H–Si substrates showed sluggish flow, thereby raising the question of the methods compatibility with all polymer film–substrate combinations. Other approaches involved using a nano-probe developed for viscosity characterization that allows temperature measurement of materials used in nano–imprint lithography polymers with submicron resolution [29].

Atomic Force Microscope, AFM was used to measure mechanical properties of a pressure sensitive polymer adhesive transfer tape [30]. The oscillation amplitude and phase of an atomic force microscope cantilever resting on an oscillating polymer surface was recorded as a function of frequency. The value of loss tangent was measured in conjunction with frequency and the measurement gave the same loss tangent–frequency dependency as that measured by macroscopic techniques. The study results sample bulk rheological properties because the contact radius is much larger than the characteristic length scales. But varying the tip geometry can help change the contact radius dimensions helping measure thin films. Thereby, the study demonstrated that AFM can measure rheological properties of thin polymeric films. However, the polymer thin film must be deformed if AFM method is to be used. A limited number of cantilever spring constants are commercially available and the probe roughness may prove stumbling blocks for potential other film measurements.

Thin film measurements of glassy systems have been studied in detail [31-36]. Cooling-rate-dependent T_g measurements were used to indirectly probe the relaxation dynamics and fragility of thin films of polystyrene. The study showed that the as the film thickness is decreased, T_g of these thin films decreases below the bulk T_g. The study demonstrated that enhanced mobility near the free surface affects the dynamics of these thin films. Surface mobility, viscosity, and T_g of thin films have been determined *in situ* through heated atomic force microscopy [34, 36] and ellipsometry [32, 33]. Using Magnetic Rotational Spectroscopy, MSR as method to probe rheology of thin films is being studied **[37]**. The idea behind MSR being, in-plane rotation of magnetic probes in a rotating magnetic field display a unique feature. The probes first rotate synchronously in unison when the rotation frequency of the applied field is increased. However, the probes undergo a transition from

synchronous to asynchronous rotation when the rotation frequency of the external field passes a characteristic frequency. This transition is dependent on the fluid viscosity. The study takes advantage of this effect and uses it to analyze viscous properties of different materials. The study demonstrates that MRS with rod-like probes provides unprecedented control over micro and nanoscale rheological measurements.

1.5 Dewetting and Rheology

Dewetting is a process where a thin liquid film on a substrate ruptures and results in the formation of droplets. The opposite of dewetting is called spreading. Spontaneous spreading and dewetting is dependent on the spreading coefficient S. If $S > 0$, spreading occurs and if $S < 0$ then dewetting occurs. For thin polymer films spun on a substrate, even if $S < 0$, dewetting doesn't occur when the temperature is below the polymer T_g. However, when the film is annealed and the temperature is increased, dewetting takes place. Dewetting can also be defined as a process where fluid flows to expose the substrate. Dewetting starts in different ways such as nucleation and growth or spinodal dewetting. In the nucleation and growth process, random nucleation of holes in the film occur does exposing the substrate to external environment. In spinodal dewetting there occurs a fluctuation in thickness and predominantly occurs in thin films. After a hole is formed on the surface, it slowly enlarges due to dewetting. The rate of enlargement depends on the boundary conditions, driving forces, and properties of the material layer and is a dynamic process. The final stage involves the fusion of many such formed holes on the material surface. Dewetting studies were conducted by annealing polystyrene films less than 100 nm thick on silicon substrates, above the T_g [38]. The study showed that thin film dewetting occurs in three stages. Initially, the films were seen to break and create

holes. The holes then grew and the rims ahead of the holes merged to form cellular structures. Finally, the resulting ribbons were seen to be unstable and decayed into droplets. The dependence of the average distance between initial holes on square of film thickness, h^2 agreed with theoretical prediction. However, the mechanism behind creation of initial holes were left unanswered. Experimental and theoretical studies were conducted to study viscoelastic dewetting of constrained thin polymer films [39]. The studies showed that the early stages of dewetting for spin-coated viscoelastic thin polymer films caused by annealing were dominated by residual stresses and nonlinear friction at the solid–liquid interface. It was showed that the residual stresses were a result of the film preparation method used, which was fast evaporation of the solvent during spin coating. Further studies demonstrated theoretical attempts to analyze profile of dewetting thin polymer films near T_g and analyze relationships between dry region radius and rim height with time [40]. Dewetting thin polymer films is a method by which viscous and viscoelastic response of polymers thin films are studied. Studies have been conducted that demonstrate measurement of hole growth in thin freely standing polymer films as a method to probe nonlinear viscoelastic effects in confined polymers [41]. The measurement was conducted using an optical microscope and exponential growth of the hole radius and uniform thickening was observed during the study. The measurements were interpreted in terms of the dependence of the viscosity on the shear strain rate associated with the hole growth process. Review studies demonstrated dewetting being a potential method to analyze and understand the rheological properties of thin polymer films [7]. Dewetting method showed that obtaining understanding between molecular scale properties and macroscopic behavior is simple. Studies conducted demonstrated the ability to understand the physics of

dewetting process by using a Newtonian fluid as a model system. Taking this approach to spin-coated polystyrene films helped study the viscoelastic properties and relaxation processes in thin polystyrene films. Significant deviations from bulk behavior was identified for films of high MW. It was also observed that the solvent quantity and the time history of the solution is important to predict the polymer thin film properties. Studies showed the aging behavior of thin films depended on film preparation conditions below T_g and the significant changes were also observed at room temperature may also potential influence a reduced T_g. However, the review study failed to propose a quality relationship between dewetting and a lowered T_g. Thus, further experiments are needed to help explain relationship between film preparation and thin polymer film properties. Further studies were conducted to determine low-shear effective viscosity of entangled polystyrene thin film melts [42]. The films had thickness range in between 27 nm to 100 nm, on Silicon Si substrates. The thin films were annealed and the method was based on the notion that thin liquid films become unstable and rupture due to defects or dewetting. It was observed that the holes created in the film grew at a rate determined by a balance between the capillary driving forces and the viscous resistive forces. It was shown that, based on the hole growth velocity, the viscosity decreased with decreasing film thickness ranging in between 25 nm and 50 nm. The observation was justified with the mobility of chain segments, which was also believed to be responsible for the apparent decrease of the T_g with decreasing film thickness. However, it was noted that the trends depend on the substrate polymer pair and cannot be generalized and interactions between polymer and substrate need to be controlled to potentially investigate relationship between η and *h.* Current thin film study methods require whole-film levels [35, 43-48]. Dewetting as a method to form patterns on polymer

surfaces has long been touted as a novel method. Experimental studies showed the ability for good quality patterning by dewetting polymer thin films [49]. Dewetting of thin films were achieved by using a combination of heterogeneous substrates, physical confinement and the movement of three-phase line. Further studies demonstrated thin polymer film dewetting as a method to pattern or functionally coat surfaces. The study demonstrated that dewetting of thin polymer films was instrumental to help study the fundamental properties and dynamics of dewetting which in turn can be tuned using the polymer viscosity [50]. Solvent annealing was used to expose the polymer to certain solvents is used to bring the polymers above their T_g, and they were studied as they dewet in real time. The advantages of patterning by dewetting was shown to be low cost, not requiring deep knowledge of film dynamics and the potential to attain a high sophistication level. Some of the disadvantages of the method were the limitation in the number of pattern shapes that could be produced and scratch stability of thin films from sharp objects.

1.6 Focused Laser Spike (FLaSk) Dewetting

Research over the past few decades have been dedicated to using laser as an approach for patterning on polymer surface. Patterning on polymer surface is achieved using the coupled forces of thermal gradients as described by the Marangoni coefficient, β.

$$\beta = \delta\gamma/\delta T \quad (1)$$

The Marangoni coefficient quantifies changes to the surface tension with temperature. In (1), γ refers to the free-surface tension of the material and T refers to the temperature. The Marangoni coefficient can then be used calculate Marangoni shear, τ [51].

$$\tau = \beta\nabla T \quad (2)$$

Focused Laser Spike (FLaSk) is high intensity method which has been used as a potential probing and imaging method. For instance, Raman spectroscopy which uses focused laser is used as a noninvasive optical method to understand molecular composition of skin [52]. Studies have been conducted to study the ability to pattern polymers using a thermocapillary approach obtained by FLaSk annealing [53] [54]. These studies utilized FLaSk annealing to create large thermal gradient around 100–750 K/μm for the dewetting of polymer thin films and the alignment and reordering of block copolymers (BCPs). In this way, it was demonstrated that thermal gradients could simultaneously provide both the mobility and driving force for assembly. higher gradients led to complete dewetting of polymer films into trench-ridge patterns [55, 56]. Dewetting of a simple polymer system (PS) using laser spike annealing was demonstrated as a process that can be used for pattern transfer of sub-micrometer lines. The method was shown to not require a development step. The study showed that the advanced patterning capability as the lines were brought together. The study demonstrated the ability to create high resolution features by resist deposition, laser patterning, and etching process thereby eliminating the necessity for wet chemical development and the possibility of removing hazardous chemicals from the lithographic process. Studies have been conducted that involved using FLaSk induced Marangoni dewetting as a method to pattern polymer thin films [55]. The mechanism of Marangoni dewetting is described by the following equation:

$$\mu \frac{dh}{dt} = -\nabla \cdot \left(\frac{h^2 \beta \nabla T}{2} + \frac{h^2}{3} \nabla (\gamma \nabla^2 h) \right) \quad (3)$$

where μ is the fluid viscosity and h is defined as the thickness of the film. The study demonstrated that polymer MW affected the linewidths. The T_g only helped determine

whether or not the substrate would be damaged before polymer dewetting. It was also observed that the only parameter that caused a significant difference in the final profile shape was the polymer film thickness. The study showed that the final film shapes all experienced the same peak temperature and thermal distribution in the simulated heating profiles. It was also observed that the dewetting was independent of surface affinity and dependent only on the MW or, equivalently, the asymptotic melt viscosity of the polymer [55]. The study finally concluded that FLaSk dewetting could be used as a highly controllable direct patterning method. Other studies have demonstrated the use of Marangoni forces for polymer surface patterning [57-60]. Finite element method (FEM) simulation studies to model FLaSk dewetting systems have also been conducted [55]**.** The thermal dependence of viscosity is a unique feature of FLaSk. FLaSk was also utilized to determine the critical cooling rate in metallic glasses which affects the glass forming ability of metallic glass [61], serve as a potential probing method. The study involved FLaSk being used in conjunction with X-ray diffraction mapping and FEM simulations.

This study seeks to use FLaSk as a method to probe rheology of thin material films. The study aims at developing a method that would help analyze and understand materials properties from the dewetting results. The aim of the study is to calculate viscosity at a specific temperature and magnitude of shear from dewetted patterns. As mentioned, previously studied dewetting methods require whole–film levels. FLaSk exists in a regime of extreme viscosity gradients. Viscosity has the ability to vary by orders of magnitude over small temperature ranges. This is where FLaSk allows for the evaluation of thin film properties in a difficult to access regime–high temperature and high shear. In addition, there is evidence that FLaSk can probe surface dynamics inaccessible to whole-film

measurements. The advantages behind using FLaSk would be its fast response and the possibility of low requirement of testing material. FLaSk experiments can be performed over very small areas, which will be extremely useful when the material in question is expensive to obtain. A single microscope image can potentially measure and supply information about multiple experimental conditions on a single film. The method will provide the ability to conduct *in situ* optical analysis while running experiments. FLaSk can provide an efficient approach to measure the rheology of thin films rapidly and locally in a high throughput fashion. Challenges faced in developing FLaSk probing methods arise primarily due to spatial and temporal variations. This study seeks to understand the potential ability to use FLaSk as probing method. The method is used to extract materials properties of three thin films of different composition, T_g and MW. The properties are extracted as a function of laser power, exposure time and laser spot intensity.

CHAPTER 2 – EXPERIMENT METHODOLOGY

2.1 Heating Substrate Preparation

Undesired antireflection effect occurs when the material on top of a doped silicon substrate is heated, as was used previously [53]. To avoid this effect, the material heating has to occur from the bottom, through the heating of the substrate as depicted in Fig. 2.1. To achieve this effect with minimal rise time and variability, a thin absorbing layer is desired to absorb the laser energy while also making sure that the substrate is thick enough to prevent the light from penetrating it. Therefore, to avoid antireflection effects and material absorption, a universal heating substrate has been designed. The heating substrate consists of a ceramic-coated optically-absorbing thin film on a transparent supporting substrate. The ceramic is used to isolate the absorber from the test material, then heat the absorber with the laser through the supporting substrate. This is done to make sure the laser does not interact with the test material. Double-side polished sapphire wafers with a thickness of 600 μm are bought from UniversityWafer. The wafers are then cleaned using acetone, isopropyl alcohol and de-ionized water (DI water) in sequence and finally blown dry using compressed air. After the wafers are cleaned thoroughly, the layers are deposited using an electron beam evaporator. Initially approximately close to 81 nm of Molybdenum, Mo is deposited at a vacuum level around 1.8×10^{-5} Torr as the absorber. This is because Mo is a thermally-stable refractory metal possesses the second highest melting point meaning it can be heated up to an extremely high temperature before it is melted. Tungsten can also be used as an alternative. Then, 6 nm of Aluminum, Al is deposited on top of the Molybdenum after which the vacuum is broken. The prepared substrate is kept under ambient condition for more than 30 days for the Aluminum layer to oxidize.

(a)

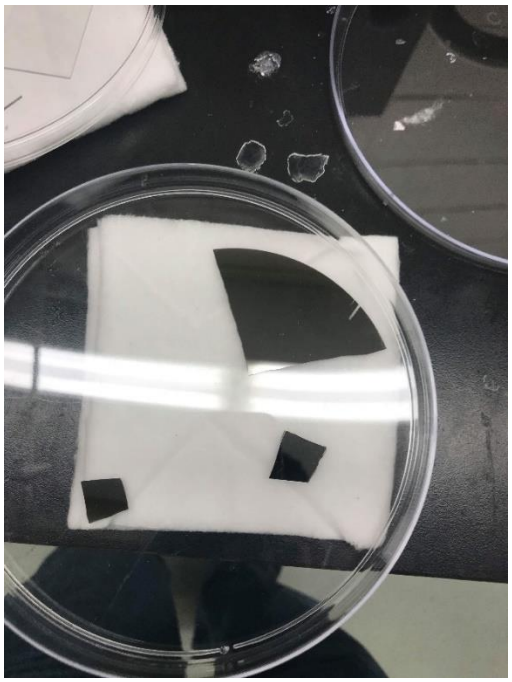

(b)

Fig. 2.1 (a) Schematic of a universal heating substrate heated from below (b) Heating Substrate–Aluminum on Molybdenum on Sapphire Wafer

2.2 Plasma Etching

To increase the affinity between the substrate and the polymer solutions, we employ plasma etching. Plasma etching is performed inside a gas chamber without the use of liquids. The substrate is placed in a vacuum chamber on the cathode of the plasma machine. Once the machine is tightly sealed, the pressure and plasma discharge parameters are selected. The machine is started after which gas or plasma is introduced to initiate the process. During

plasma etching, the gas introduces very reactive species that react with the substrate surface and causes the substrate surface material to break down into very small particles which are then removed by the vacuum system. An important requirement in plasma etching is the need for the by-products to be able to evaporate away into the pumping system. If not, the by-products will remain on the substrate resulting in an undesired film. Once the plasma etching and vacuum pump down is completed, the substrate is removed from the chamber and used for the spin coating process.

2.3 Polymers

Three thin films were prepared during the course of this study. Materials used to prepare the thin films were Polystyrene (PS), Poly4–hydroxystyrene (PHS) and N, N′-Bis (3–methylphenyl)–N, N′-diphenylbenzidine (TPD). The first two are polymers and the last one an organic molecule. The PS used had weight averaged MW equal to 35000 kg mol^{-1} and the PHS used had weight averaged MW equal to 25000 kg mol^{-1}. Individual 5 % solutions by weight were made for them by dissolving the polymers individually in Propylene glycol monomethyl ether acetate (PGMEA). The TPD used had weight averaged MW equal to 516.67 kg mol^{-1} and likewise a 5 % solution by weight was made by dissolving the molecule in Dichlorobenzene (DCB). Since the study is being conducted to calibrate the heating substrate and get a power–intensity–temperature relation, materials whose properties are well understood are needed. The three materials chosen are well studied in the material science field. PS is a polymer system that has been extensively studied and the dependence of its T_g on surface and thickness is well known [62-65]. As mentioned previously, T_g of glassy thin films are extremely sensitive to the nature of the surface and even in this case, Polystyrene thin films are studied the most [7-10]**.** TPD is a

molecule that is well studied [36]. TPD as mentioned above, is a small molecule whose MW and chain length are smaller when compared to the polymers – PS and PHS. PHS has MW nearly in the same range as PS, but the T_g and, therefore, viscosity at a given temperature is different from PS.

2.4 Spin Coating Process

One of the most common ways to produce a thin uniform continuous polymer film on a substrate is by utilizing the method of spin coating. Spin coating process is frequently employed in the semiconductor and microelectronics industry to produce photoresists. Spin coating is categorized into four key stages – Solution deposition, rapid acceleration, steady spin and evaporation drying. In the spin coating process, the heating substrate is first attached firmly onto a vacuum chuck. In cases where the heating substrate is smaller than the vacuum chuck surface area, the substrate is temporarily attached to a Polydimethylsiloxane (PDMS) coated glass slide and this in turn is attached to the vacuum chuck. The PDMS acts as a mild but effective adhesive. Once the substrate is firmly secured, the dilute polymer solution is first deposited on the substrate using micro syringes. The solution is deposited either on the entire substrate surface or around the center of the substrate surface. Then the substrate is rapidly accelerated to the desired spin rotation rate (RPM). Here the polymer solution flows radially as a result of the centrifugal force action. The excess of the deposited solution is thrown off the edge of the substrate. When the substrate is spinning at a constant rate for a specified time, the fluid viscous forces dominate the thinning behavior. The remaining solution begins to thin slowly until it reaches an equilibrium thickness due to fluid forces and pressure which affects the thickness of the final layer. Once the steady spin stage ends, the film begins to dry. In this stage the

centrifugal force that pushes the solution outwards stops and the film potentially thins due to solvent loss. The spin-coated substrate is then baked on a hot plate for a few minutes at a temperature below the polymer T_g. This results in a rise in viscosity due to evaporation of residual solvent. Baking ensures that the final thinning of the spin-coated film is solely a product of solvent evaporation. It has been experimentally determined that an increase in the spin rotation rate will decrease the film layer thickness. However, there has been difficulty in the attempts to mathematically model the relations between rotations per minute and rotation time to the final thickness of the layer due to the complexities involved in fluid rheology and solvent evaporation. Spin coating has advantages in that the film thickness can be easily changed by changing speed and it is low cost and fast operating. However, the biggest disadvantage is the very low solution utilization efficiency as a lot of the deposited solution is thrown off the substrate and wasted.

2.5 Film Thickness Measurement

Once the spin coating process is completed the thickness of the resulting polymer film is measured with the help of Filmetrics F40 device. Thin film measurements are traditionally performed using optical and stylus-based techniques. Stylus measurements monitor deflections of a fine-tipped stylus on the film surface and uses this information to measure film thickness. Optical techniques determine thin-film characteristics by measuring how the films interact with light. Optical techniques are advantageous as they are accurate and cause no damage to the polymer film. The Filmetrics F40 device analyzes and measures single layer and multilayer film thickness using spectroscopic reflectometry. The Filmetrics F40 device uses an internal light source – a tungsten–halogen bulb which generates light in the 375 nm to 3000 nm wavelength width. Light is sent to the polymer

film and the reflected light is collected with the help of fiber optic cables and lens. The intensity of this light is measured at various wavelengths using a spectrometer. The spectrometer splits and diffracts light into various beams with the help of a diffraction grater and measures the light at different wavelengths using photodiodes. Thin film measurement depends on two major optical constants – Film refractive index, η and extinction coefficient, *k*. Refractive index is defined as the ratio of speed of light in vacuum to the speed of light in the material. Extinction coefficient is a measure of how strongly a substance absorbs light at a particular wavelength. The measurement also depends on wavelength, λ and the distance the light travels, *x*. When light is focused on a multilayer film, it gets reflected from the top and bottom surfaces of a thin film. The reflections from the two surfaces depict wave nature and may add up together constructively or subtract each other destructively based on their phase relationship. The phase relationship is determined by film thickness *x*, optical constants – η and *k*, wavelength λ and difference in optical path lengths of the two reflected lights. This results in intensity oscillations in the reflectance spectrum arising as a characteristic of the film. Filmetrics measures the amplitude and period of the oscillations and determines the thickness of multiple thin films. FILMeasure analyzes and calculates a reflectance spectrum that is close to the measured reflectance spectrum of the film in question, and this is used to determine film thickness. For this process, FILMeasure requires the user to input sample film structure data and an initial guess for thickness along with thickness constraints. FILMeasure varies parameters until the calculated reflectance spectrum is close to that of the measured film reflectance spectrum by searching through a range of acceptable thickness values based on the initial

thickness guess. The calculated and measured spectra is analyzed using either curve fitting or Fourier transform method and the best possible match results in the final thickness.

The device was mounted on an optical microscope. Initially the microscope lamp was turned on and allowed to stabilize for a few minutes, otherwise known as “warm-up” time. The device uses the optical microscope camera to focus on the film surface. A baseline measurement is performed to calibrate the FILMeasure software to determine the system spectral response. This is performed by measuring a reflectance standard with known reflectance characteristics. The sole purpose of baseline measurement is to calibrate the device and therefore it is not necessary for the reflectance standard to be the same substrate on which the polymer film is deposited. To obtain baseline measurement a clean silicon, Si wafer of known thickness was placed on the microscope stage, a clean area was chosen and focused on using the microscope controls. Baseline measurement was selected in the FILMeasure software and the sample reflectance measurement results in a plot that depicts reflectance versus wavelength with peaks and troughs. The reflectance standard of the background was measured by focusing light on a 45-degree angled reflectance substance on the microscope stage. The reflectance substance is replaced by the Si wafer and the thickness is measured. The obtained thickness value should be ideally close to the known wafer thickness and the fit value is ensured to be good to complete the reflectance reference standard measurement. This concludes the calibration process for the device. The edit recipe option is used in the FILMeasure window to input the material characteristics of the polymer thin film layer and substrate and the hypothetical film thickness value. The substrate and all film layer materials are chosen from the material library and the corresponding reflective indices are manually entered if required in the edit recipe option

in the FILMeasure software. Finally, the polymer film is loaded on the stage and the thickness is measured. The polymer film is then loaded on the microscope stage and focused on and the thickness is measured. The obtained thickness value is the polymer thickness value and the fit value is ensured to be good, at least 90% to ensure accurate measurement. To obtain an average value of the film thickness, mapping is performed by using a custom-built Python program in co-ordination with the Filmetrics device.

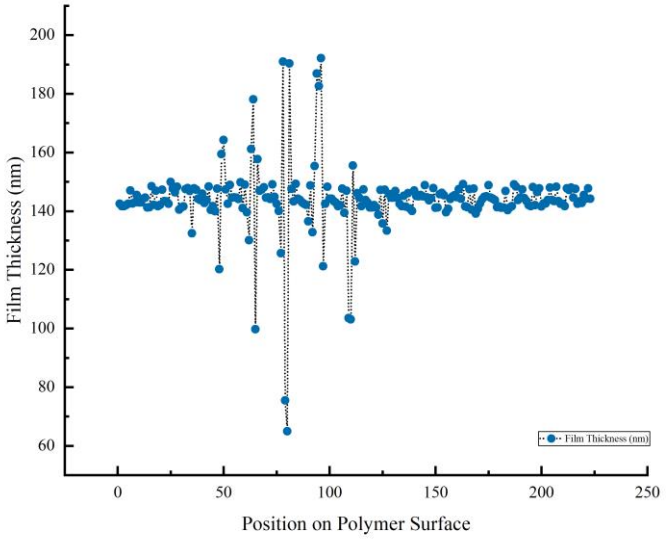

Fig. 2.2 Film thickness map of thin Polystyrene (PS) film on heating substrate

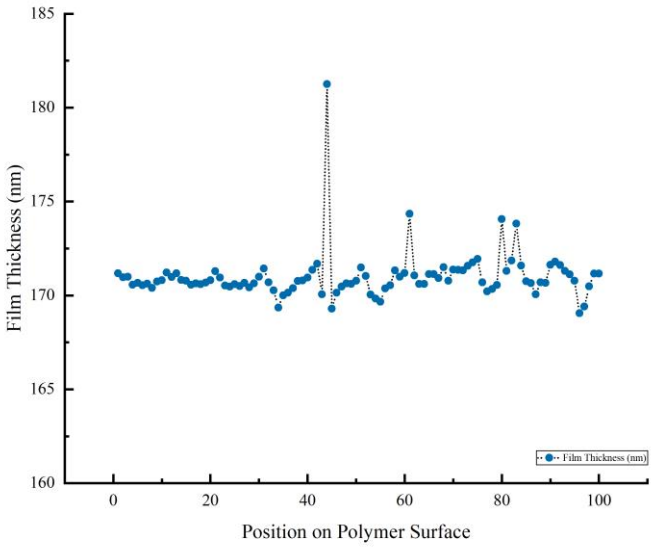

Fig. 2.3 Film thickness map of thin Poly–4–hydroxystyrene (PHS) film on heating substrate

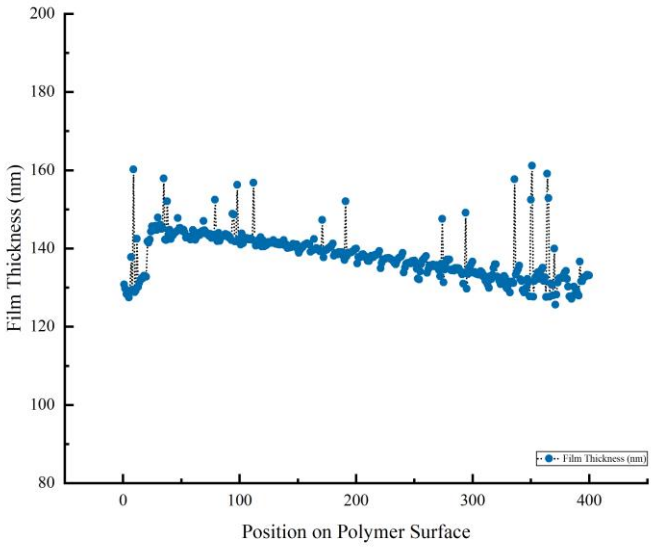

Fig. 2.4 Film thickness map of thin N, N′-Bis (3–methylphenyl)–N, N′-diphenylbenzidine (TPD) film on heating substrate

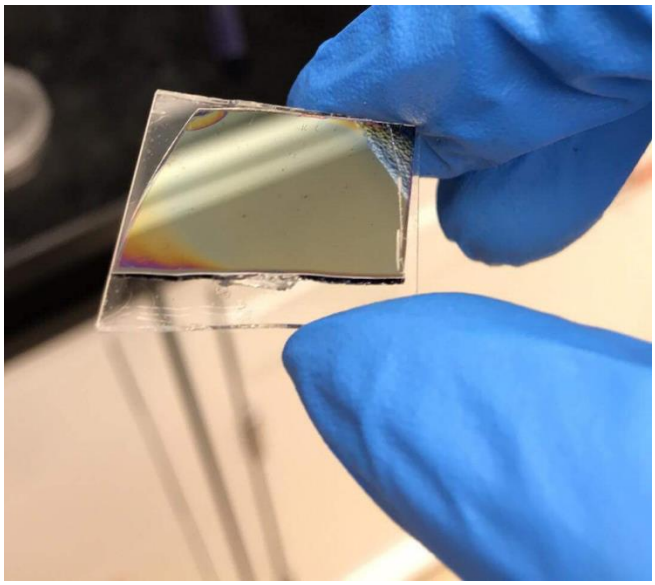

Fig. 2.5 Thin Polystyrene film on heating substrate

As observed from the Filmetrics film thickness mapping shown in Fig. 2.2, Fig 2.3 and Fig. 2.4, it was observed that PS film had an average thickness of 153 nm on measuring 225 points measured over a 22500 μm^2 area. PHS film had an average thickness of 174 nm on measuring 100 points over a 10000 μm^2 area and TPD film had an average thickness of 142 nm on measuring 400 points over a 40000 μm^2 area

2.6 FLaSk Setup

Patterning on the thin film polymer is conducted with the help of a custom-built laser apparatus. The thin film polymer samples are mounted on MCL-MOTNZ integrated nano-positioning and micro-positioning stage which has a resolution of 95 nm. The polymer film samples are placed such that they facing the free-space FLaSK objective. Excitation is provided by an opus 532 nm continuous wave diode-pumped solid-state laser. Power is controlled by using an ISOMET IMAD-T110L-1.5 acousto-optic modulator (AOM). The modulator is controlled by a NI-9263 data acquisition board with custom MATLAB

software. Power is monitored using a Thorlabs power meter and a partially reflective mirror in the beam path. The patterning is conducted at manually-implemented focus. The polymer thin film is on top of a thin heating substrate which then lies on top of a transparent substrate like borosilicate glass, fused quartz or sapphire as shown in Fig. 2.7.

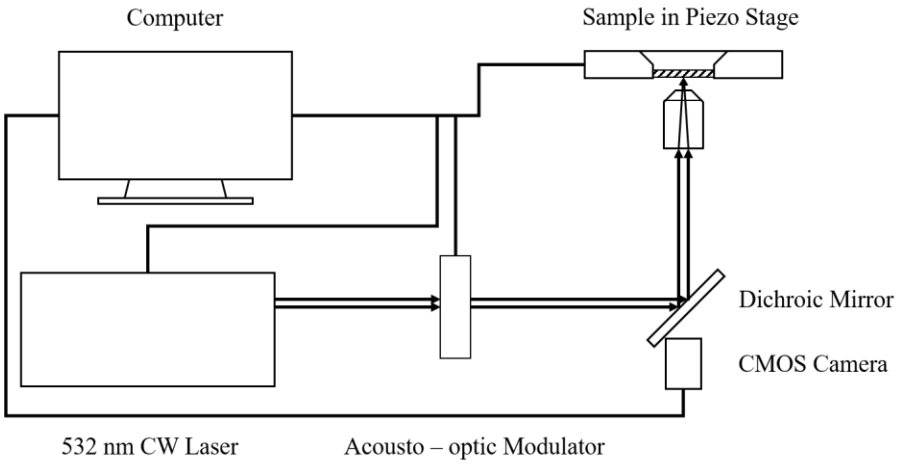

Fig. 2.6 FLaSk system setup

As shown in Fig. 2.6, the laser system has a 532 nm continuous wavelength laser source. The laser emitted by the laser source then goes through an AOM which serves as a

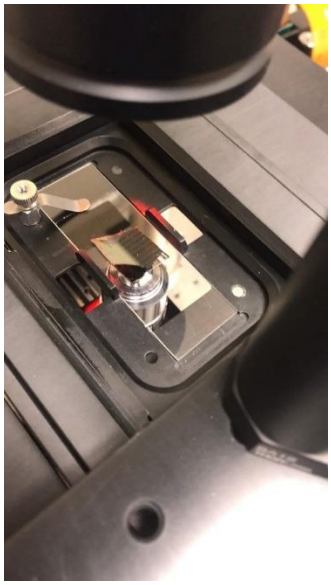

Fig. 2.7 FLaSk setup

shutter that can control the power and the exposure time. The laser power is tracked and calibrated using a power meter.

The system behavior is controlled by a MATLAB program and has a time resolution smaller than 0.1 ms. The numerical aperture, NA of the lens used in this study is 0.25. The FLaSk system performs a dot exposure which is tunable in exposure time and power as opposed to transferring the laser spot on the polymer film in the work done by. The focusing of the laser spot on the polymer and the video of the annealing process required to calculate intensities is performed using Thorlabs DCx camera. The camera frame rate is held at 15.63 Hz and the camera exposure time is held at 7.37 ms.

2.7 FLaSk Program

The laser is focused onto the heating substrate manually and the exposure program, which is automated, is run using the custom-built MATLAB software. The program is a dot exposure program that opens the shutter, tunes to the specified power, runs for the specified exposure time and finally closes the shutter. The power ranges and exposure times are determined based on the dewetting characteristics of the film. The focus then moves to the next point in accordance to the program. The dot exposure pattern is in the form of an array with columns accounting for the laser power and the rows accounting for exposure time as observed in Fig. 2.8.

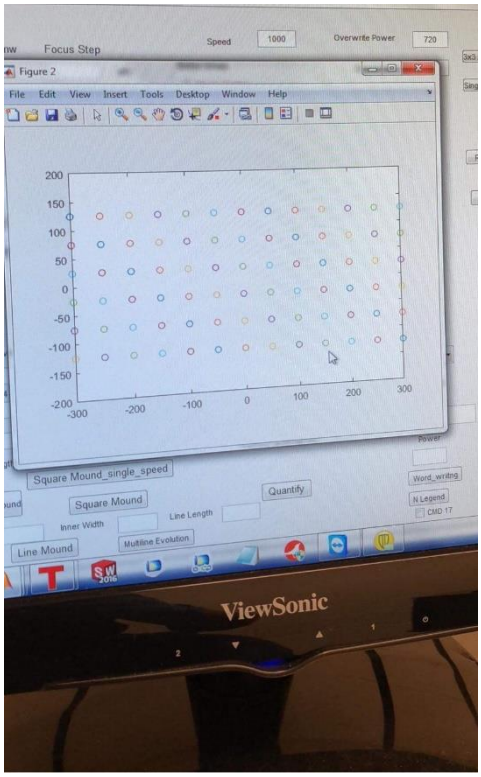

Fig. 2.8 Dot exposure program pattern preview in MATLAB

Fig. 2.9 FLaSk dewetting process as observed through Thorlabs DCx camera

The laser power and exposure times chosen during the FLaSk dewetting process of each material is as follows. Polystyrene film experiments were conducted with laser power

ranging from 5 mW–85 mW in steps of 5 mW and exposure time equal to 10^{-x} sec, with x ranging from 0 to 5 in steps of 1. Poly–4–hydroxystyrene film experiments were conducted with laser power ranging from 50 mW–110 mW in steps of 5 mW and exposure time equal to 10^{-x} sec, with x ranging from 1 to 4 in steps of 1. Finally, TPD film experiments were conducted with laser power ranging from 20 mW–60 mW in steps of 2 mW and exposure time equal to 10^{-x} sec, with x ranging from 0 to 5 in steps of 1.

2.8 Imaging

After FLaSk dewetting, Leica Microsystems Optical Microscope DM 2700 M was used to image the substrate coated with thin films. The microscope was used to observe the dewet pattern and also obtain images of the dewet spots under high magnification. These images were used for further analysis.

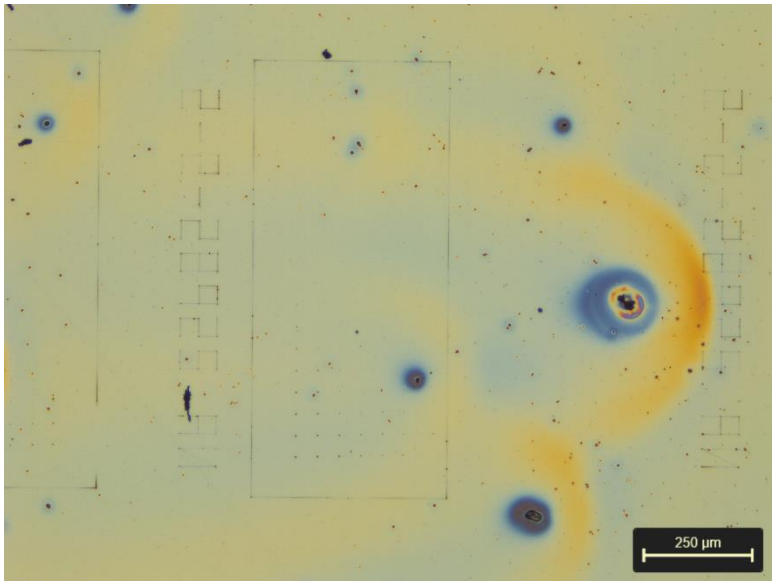

Fig. 2.10 Polystyrene (PS) film dewet pattern image 5x magnification

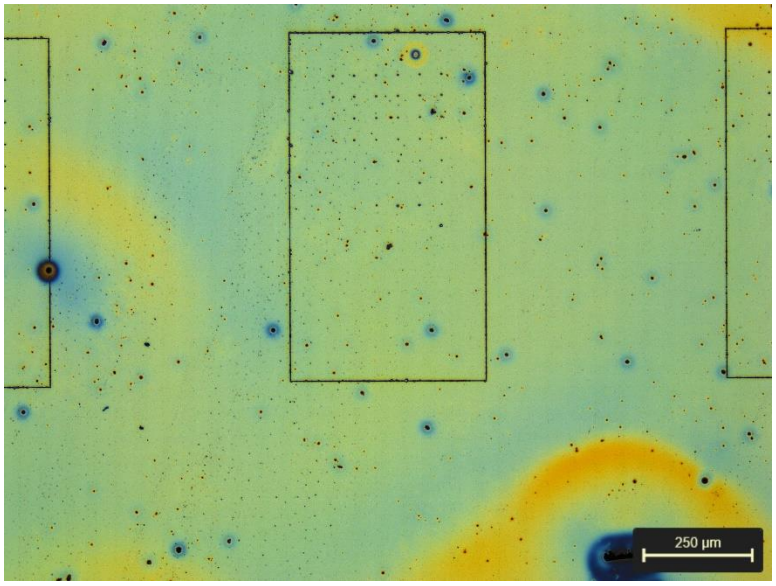

Fig. 2.11 Poly–4–hydroxystyrene (PHS) film dewet pattern image 5x magnification

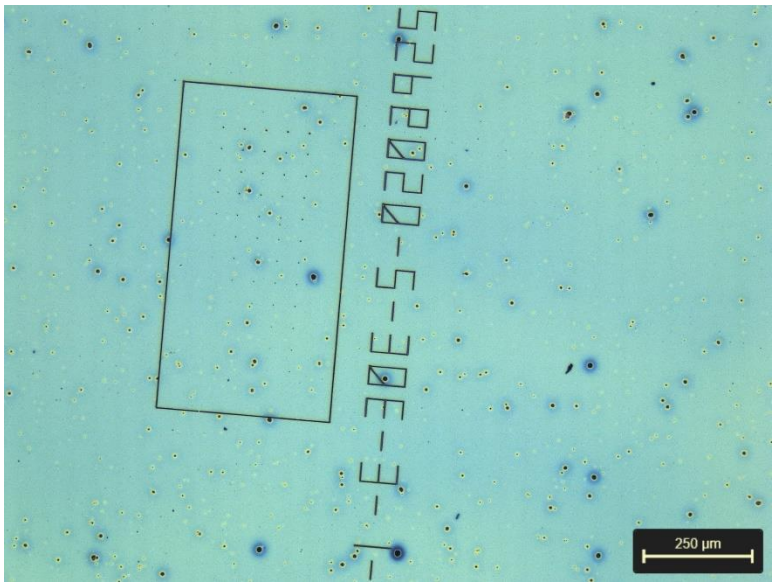

Fig. 2.12 N, N′-Bis (3–methylphenyl)–N, N′-diphenylbenzidine (TPD) film dewet pattern image 5x magnification

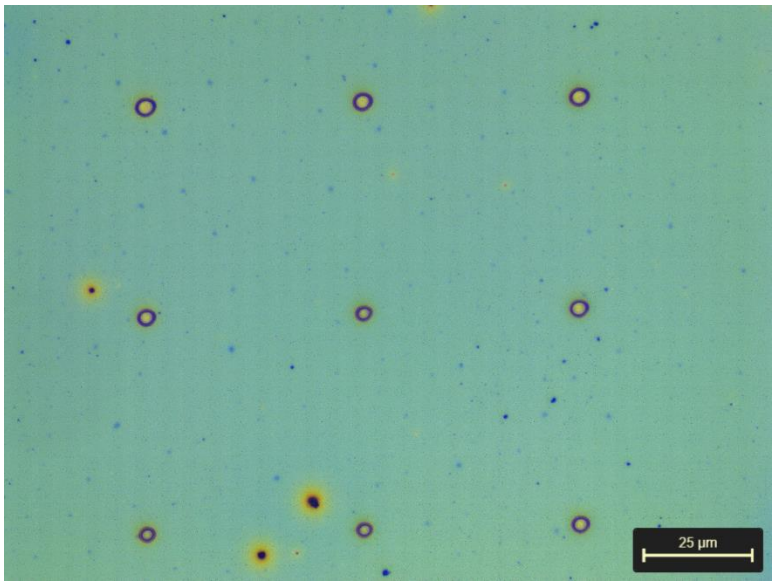

Fig. 2.13 Poly–4–hydroxystyrene (PHS) film dewet pattern image 50x magnification

2.9 MATLAB Image Processing

Image processing is the method of manipulating and modifying an existing image to get an improvised image or obtain fruitful and important information from the image. It is a branch of signal processing where the input is an image and the output may be either an image or some features of the image. The steps involved in image processing are importing the image, analyzing the image and finally obtaining necessary information from it. Image processing can be broadly classified into analogue and digital image processing. This study involves the use of digital image processing.

Each color on an image is depicted by three numerical values. The numerical values depend on the color system which is divided into either an additive color system or a subtractive color system. Each color system has a corresponding algorithm. Additive color system which is our area of interest primarily consists of three colors – red, green and blue. These three colors are added to create new colors. This color system is more commonly known

as the RGB color system. In an image, each pixel is represented by three numerical values otherwise known as intensity values in brackets. First value in the bracket represents the red intensity, the second represents the green intensity and the third represents the blue intensity. Varying the three intensity values results in different colors. The RGB values range from 0 to 255. For instance, an RGB triplet value of [0, 0, 0] results in a black color while a triplet value of [255, 255, 255] results in a white color.

An understanding of image properties and colormaps is essential to perform image processing. The essence behind choosing a colormap is to find out a good method to represent an image to extract all necessary data from the image. Colormaps used in this study are grayscale and binary colormaps. A grayscale image is one where shades of gray are the only possible colors. Binary image is one where pixels have only one of two allowed intensity values – 0 and 1 or 255. As mentioned earlier, 0 represents black and 1 or 255 represents white. A binary image is displayed as black and white image.

MATLAB was chosen as the computing environment in this study for image processing owing to its ability to handle images and videos, numerical accuracy and in-built algorithms and toolboxes. The MATLAB Image Processing Toolbox was utilized in this study. One of the major functions used from the toolbox where impixel that returns the intensity values for a certain set of pixel coordinates in a particular image. The other major function utilized was rgb2gray that converts a truecolor RGB image to grayscale image by selectively eliminating color and saturation.

2.9.1 Dewet Spot Center Identification

The study aims at understanding the influence of intensity, temperature, radius and the rheological values of materials. Red intensity values which is the luminescence of the Mo film layer**,** shown during the dewetting test is a direct indication of the local temperature [66-68] and hence the study aims to detect the red intensity value of the brightest pixel of the laser spot. Intensity of the brightest pixel of the laser spot in the image was detected in two steps – image identification and image postprocessing. The first step involves extracting all the images otherwise known as frames from the dewetting test video. The extracted frames will consist of images that contain laser spots and images that have no laser spot. The no laser spot images correspond to the instances when the polymer film is no longer exposed to the laser because the laser shutter is closed due to the end of exposure time and the stage moves according to the laser program. These images need to be discarded as they are not of interest. In order to accomplish this, an image that consists of the laser spot is selected at random and fed into the MATLAB program.

Fig. 2.14 Laser spot on material surface as captured by camera during FLaSk dewetting process

The original image is converted into a grayscale image and the zone of interest – laser spot is chosen. Fig. 2.14 shows the laser spot with the help on an arrow. Four random pixels in this region are chosen as close as possible to center and the corresponding pixel co-ordinates referred to as A, B, C and D are stored. Then all the images from the dewet test are fed into the program and for each image, the intensity values of the same four pixels A, B, C and D are analyzed. If the intensity values of the red channel of these pixels are between 0 and 5, then the image is deemed to not have a laser spot and is no longer required. If not, the image has a laser spot and are extracted and classified according to power and exposure time.

Once the necessary images are isolated, the actual work – which is calculating the highest intensity of the illuminated spot for a specific laser power, can be performed. In order to accomplish this, all the images in each power bracket is fed into the MATLAB intensity

analysis program. Each image is converted into a grayscale image as shown in Fig. 2.15 and the zone of interest – laser spot is magnified as shown in Fig. 2.16. One pixel is chosen as close as possible near the center of the spot and a 15-pixel x 15-pixel area is automatically called that encompasses the chosen pixel. The program then converts the image back into truecolor and the red intensity value for all the pixels in the 15-pixel x 15-pixel area is calculated individually.

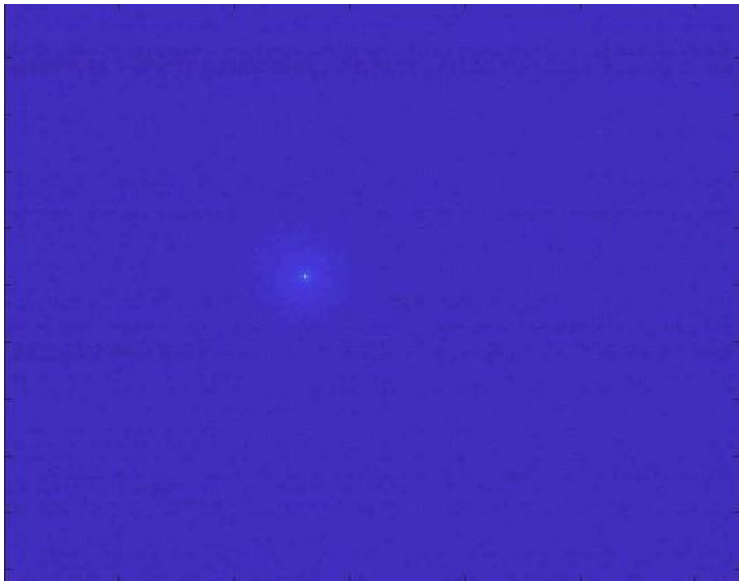

Fig. 2.15 Grayscale image of the laser spot during the FLaSk dewetting process

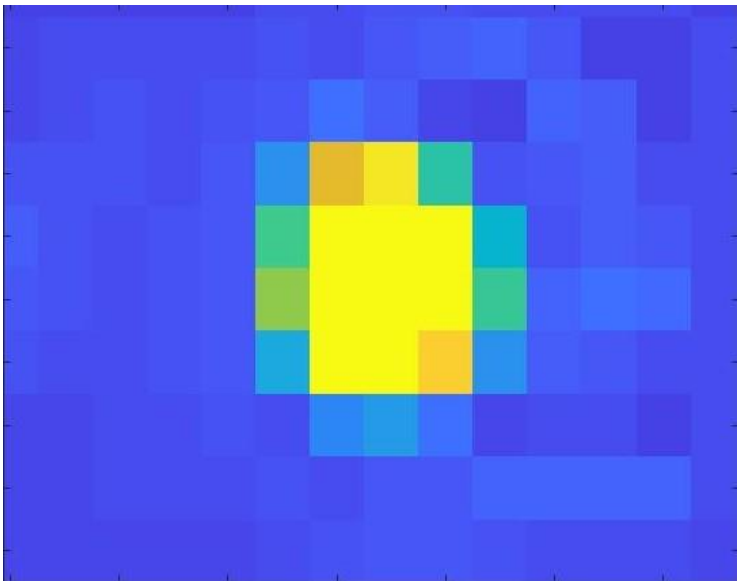

Fig. 2.16 Zoomed grayscale image of laser spot center during the FLaSk dewetting process

The highest intensity value returned by the calculation is the highest intensity value of the image. This is repeated for all the images in the power bracket. Intensity value for each image in the power bracket is stored in a matrix. The highest intensity value in the matrix is the highest intensity value for the power bracket and standard deviation for the intensity values is also calculated. The entire operation is repeated for all the power brackets and the highest intensity values along with standard deviation for each power bracket is returned.

2.9.2 Dewet Spot Radius Measurement

After performing FLaSK dewetting process on the polymer thin film, a new film profile is obtained that corresponds to a trench shape having three radii values – R_1, R_2 and R_3. It is also observed that the trench shape and radii values vary in a systematic way with the laser exposure time and power. The difference in radii values can be observed with an optical microscope. This systematic variation in R_1, R_2 and R_3 with laser exposure time and power

is of major interest as the radii values have the potential to serve as rheology measurement characteristics. Therefore, it is necessary to develop a method to calculate their values.

Once again, MATLAB was chosen as the computing environment to measure the radii of the dewet spots. The three radii of the dewet spot in the microscope image was detected by first identifying the center of the dewet spot and then calculating radii by marking edges. After the FLaSK dewetting process is completed, multiple images of the array of dewet spots are taken at different magnifications using an optical microscope. The images are categorized according to laser power and exposure time. The images are then fed into the MATLAB program.

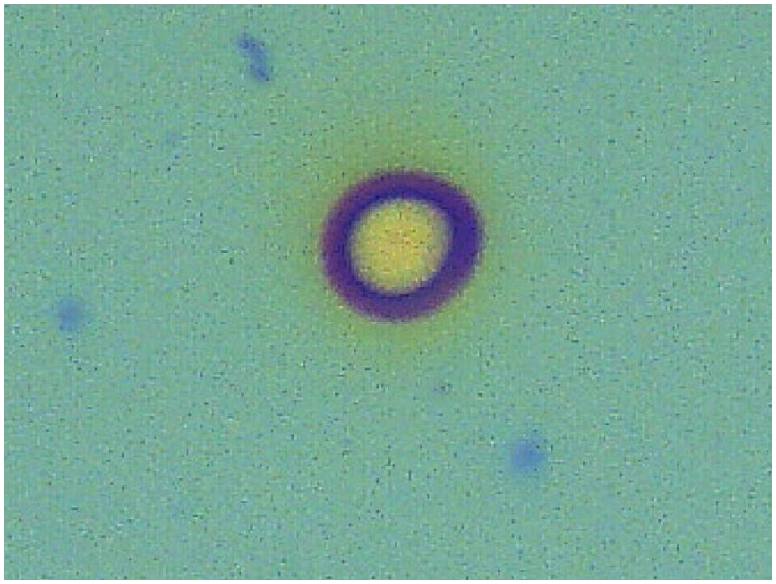

Fig. 2.17 Zoomed in microscope image of dewet spot on PHS film

The microscope images have a defined length scale while the program uses pixel distance to calculate length. Hence, the next step is to scale the length measurement in the program

to the microscope image scale. This is performed by cropping the scale bar from the microscope image and converting it into a binary image shown by Fig. 2.18. The number of white pixels in the scale is counted and then the scale length value is manually obtained from the user. The ratio of the above two quantities is the required new radii measurement scale.

Fig. 2.18 Binary image of scale bar obtained from dewet spot microscopic images

Once the new scale is calculated, the center of the dewet spot is identified. This is obtained by two methods, first the user is required to manually select three points from the visible rings and the center is calculated using the circle equation.

$$x = \frac{(x_1^2+y_1^2)(y_2-y_3)+(x_2^2+y_2^2)(y_3-y_1)+(x_3^2+y_3^2)(y_1-y_2)}{2(x_1(y_2-y_3)-y_1(x_2-x_3)+x_2y_3-x_3y_2)} \quad (4)$$

$$y = \frac{(x_1^2+y_1^2)(x_3-x_2)+(x_2^2+y_2^2)(x_1-x_3)+(x_3^2+y_3^2)(x_2-x_1)}{2(x_1(y_2-y_3)-y_1(x_2-x_3)+x_2y_3-x_3y_2)} \quad (5)$$

where (x_1, y_1), (x_2, y_2) and (x_3, y_3) are the coordinates of the three user selected points and (x, y) is the center of the dewet spot.

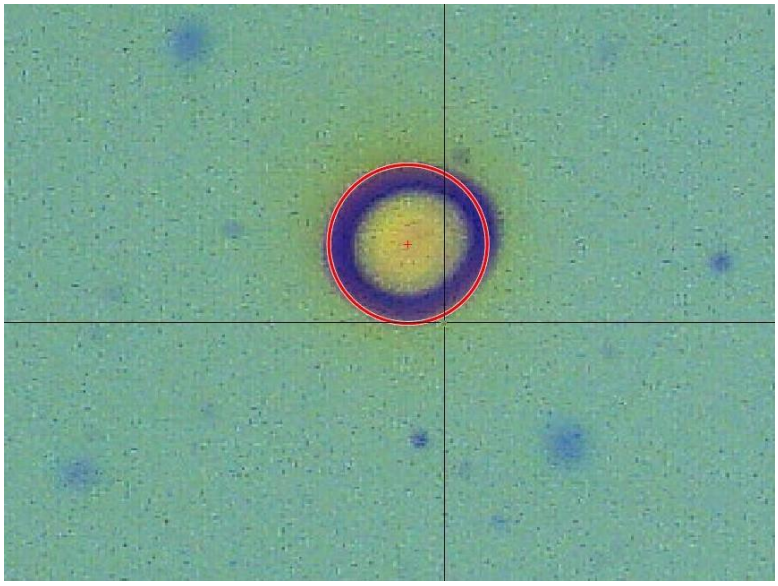

Fig. 2.19 Dewet spot center identification using circle equation method

The second method calculates the center of the dewet spot based on average pixel intensity values for RGB channel after removing background pixels and noise. The user inputs an image of the dewet spot and then selects a background region. Background region are those regions which are not a part of the dewet spot. Ideally, the software will set all pixels in the background region to 0 – Black, essentially subtracting the background. The average intensities and standard deviations of the red, green, and blue pixel intensities within the selected background region are then displayed to the user. The image is then split into its respective red, green, blue channels and displayed. The user enters a tolerance value for each channel.

The software then sets all pixels in one channel with the same value as the average background intensity for that particular channel to 0. The tolerance is the plus or minus intensity value to include in the background subtracting. For instance, if the average blue

intensity of the selected background region is 158 and the tolerance is chosen to be 0, then only those pixels with an intensity value of exactly 158 in the blue channel will be set to black. If the tolerance is 15, then all the pixels inclusively between 143 and 173 in the blue channel will be set to black. The user can use the displayed standard deviations of the average background intensities within the selection region to pick a tolerance. Another possible way of choosing a tolerance is to use trial–and–error method and keep incrementing the value until all pixels in the background region appear to be black. This must be repeated for each channel – each channel will have a different tolerance value. Once a tolerance has been chosen and the background region has been subtracted, the software performs a weighted center-finding algorithm.

The weighted center-finding algorithm can be equated to a center of mass problem, where each pixel intensity value takes the role of mass. The unweighted center-finding algorithm is the same, but treats each pixel as though they all have the same intensity value. The red, green, and blue centers are shown on each of their respective background-subtracted images, as well as the full color droplet image as shown in Fig. 2.20.

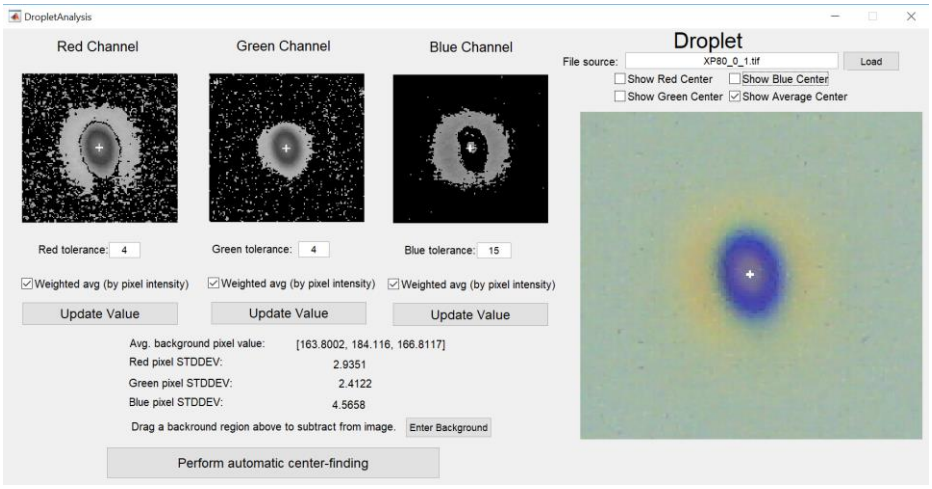

Fig. 2.20 Dewet spot center identification using pixel intensity method

Once the center-finding algorithm has been performed on each of the three channels, the average center is displayed on the full color droplet image. While both the methods produce similar results, keeping intone with the assumption that the dewet spot is a circle, this study utilizes the first method to identify the dewet spot center. After the center is identified, the user is required to manually select multiple points on the three ring edges. Selection of points results in a circle being superimposed on the spot edge. The radii are calculated by taking the average of the point distances from the center and scaling it with the radii measurement scale.

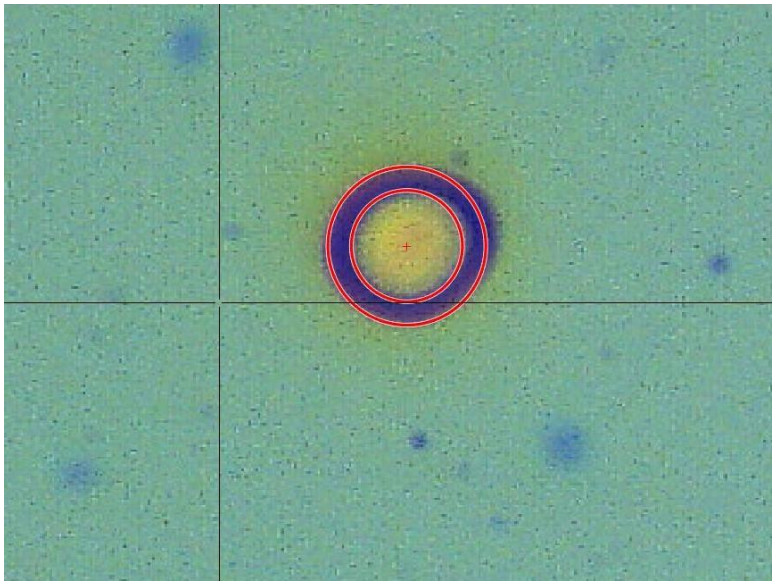

Fig. 2.21 Dewet spot with radii – R_1 and R_2

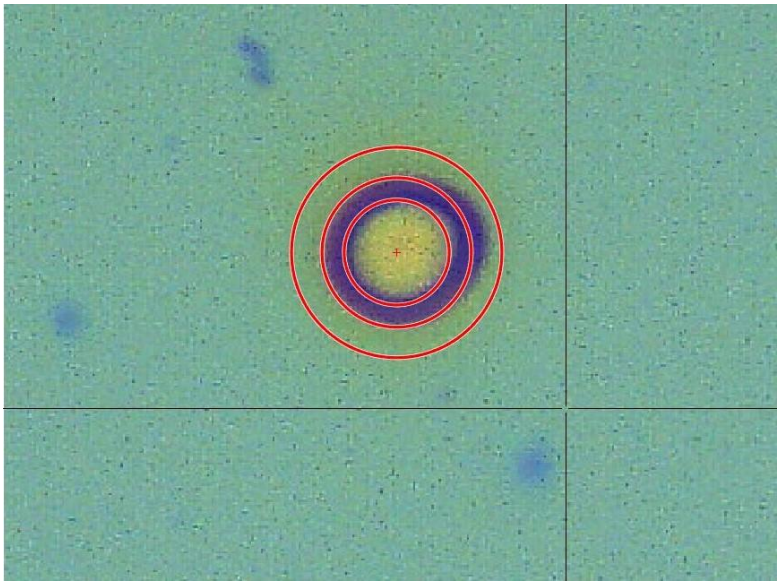

Fig. 2.22 Dewet spot with all three radii – R_1, R_2 and R_3

Multiple points are required to calculate variance in the radii. The three radii values R_1, R_2 and R_3 are recorded with the laser power, exposure time, and red intensity value. The experiments performed covers different range of observed intensities. The intensities remain consistent within a set. The results are quantified by defining the three previously

mentioned quantities – R_1, R_2, and R_3, also defined by Fig. 2.23. R_1 is defined as the radius of the highest gradient and this corresponds to the minimum reflectance. R_3 is defined as the maximum radius of dewetting and this corresponds to the edge of visible dewetting. R_1 and R_3 are easily observed optically and they can be analyzed and calculated using a pixel–color gradient program. On the other hand, R_2 is defined as the highest point of the profile and this can correspond to many different colors depending on the total thickness, making it difficult to analyze. Ideally, we would also be able to measure the slip length, R_0, but it is too difficult to observe and is negligible under the assumption of low or no slip occurring.

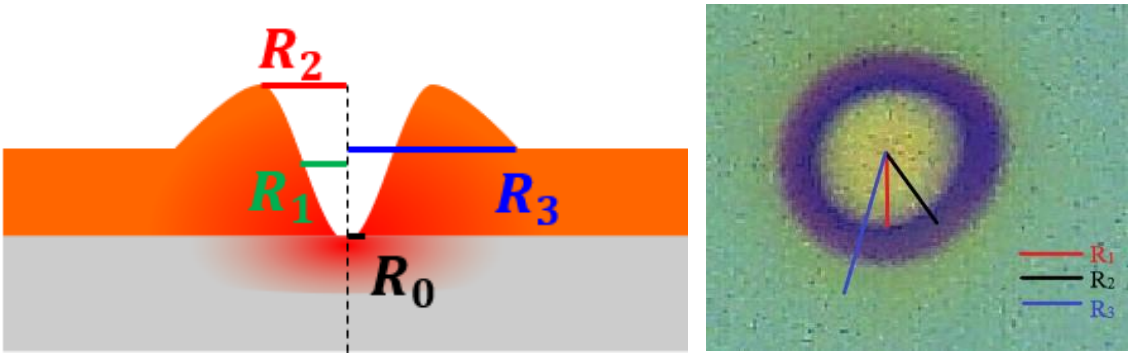

(a) (b)

Fig. 2.23 (a) Schematic and (b) optical image of dewetted PHS spot with characteristic radii indicated

CHAPTER 3 – RESULTS AND DISCUSSIONS

3.1 Approach and Preliminary Analysis

The continuous nature of viscosity in a glass transition makes glassy molecule and polymeric systems as the best model system to study dewetting. The continuous nature of viscosity allows dewetting properties to be characterized as continuous functions of temperature. Studies conducted have viscosity modeled as following the Williams–Landel–Ferry (WLF) empirical relation [11, 69].

$$\mu(T) = \mu_0 \cdot exp\left(\frac{-C_1(T - T_g)}{C_2 + T - T_g}\right) \quad (6)$$

C_1, C_2 and μ_0 are empirical parameters. Mathematics from the WLF equation suggests that viscosity can vary over orders of magnitude near the T_g and in cases sufficiently above the T_g the viscosity will approach a constant value. This in conjunction with (1) and (2) can result in three regimes of behavior for FLaSk dewetting characterized by T_g and ∇T. This study involves dewetting process with peak temperatures near the T_g and low ∇T. Dewetting here is will be dominated by the highest local temperature on the film, which is at low shear, at short time periods and can be initiated by a low numerical aperture FLaSk.

Laser power and intensity values corresponding to laser exposure time of 1 second are plotted for PS, PHS and TPD thin films. The trends are compared to understand the relation between intensity and laser power.

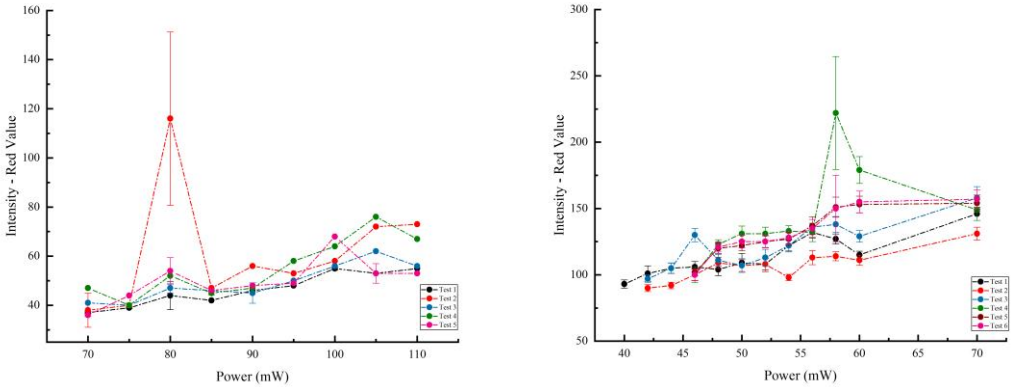

(a) (b)

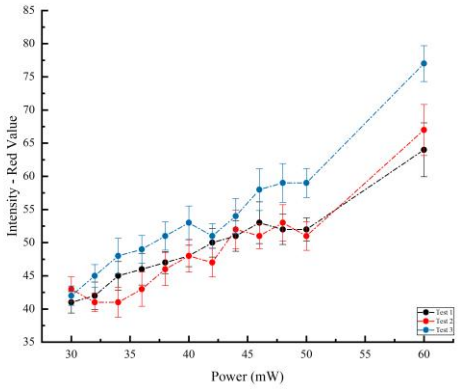

(c)

Fig 3.1 Laser spot intensity versus laser power for (a) PHS, (b) PS and (c) TPD at 1 sec exposure time

From Fig. 3.1 it is observed that intensity corelates with laser power linearly. It also observed that the intensity values are relatively consistent within a particular set. The plots

display different intensity values corresponding to the same power across the materials. This suggests that material characteristics influence intensity and the material is being directly heated. As mentioned earlier, direct material film heating is undesired as to avoid anti reflection effect. This apparent deviation in intensity is inconsistent with expectations, since the material thermal characteristics are negligible when compared to thermal characteristics of the selected heating substrate. The trends however demonstrate that at the 1 second exposure time all the materials have the same dewetted profile. Therefore, for the study it is assumed that intensity varies only with localized temperature and as mentioned is an indicator of local temperature. Also, the material effects can be neglected. The variation in intensity of different materials across the same power can be attributed to variation in experimental conditions such as focusing of the laser and multiple laser alignment and realignments that occurred during the course of experiments. Next for preliminary analysis laser power and radii values – R_1 and R_3 corresponding to laser exposure time of 1 second are plotted for PS, PHS and TPD thin films. The trends are compared to visualize the relation between dewet spot radius and laser power.

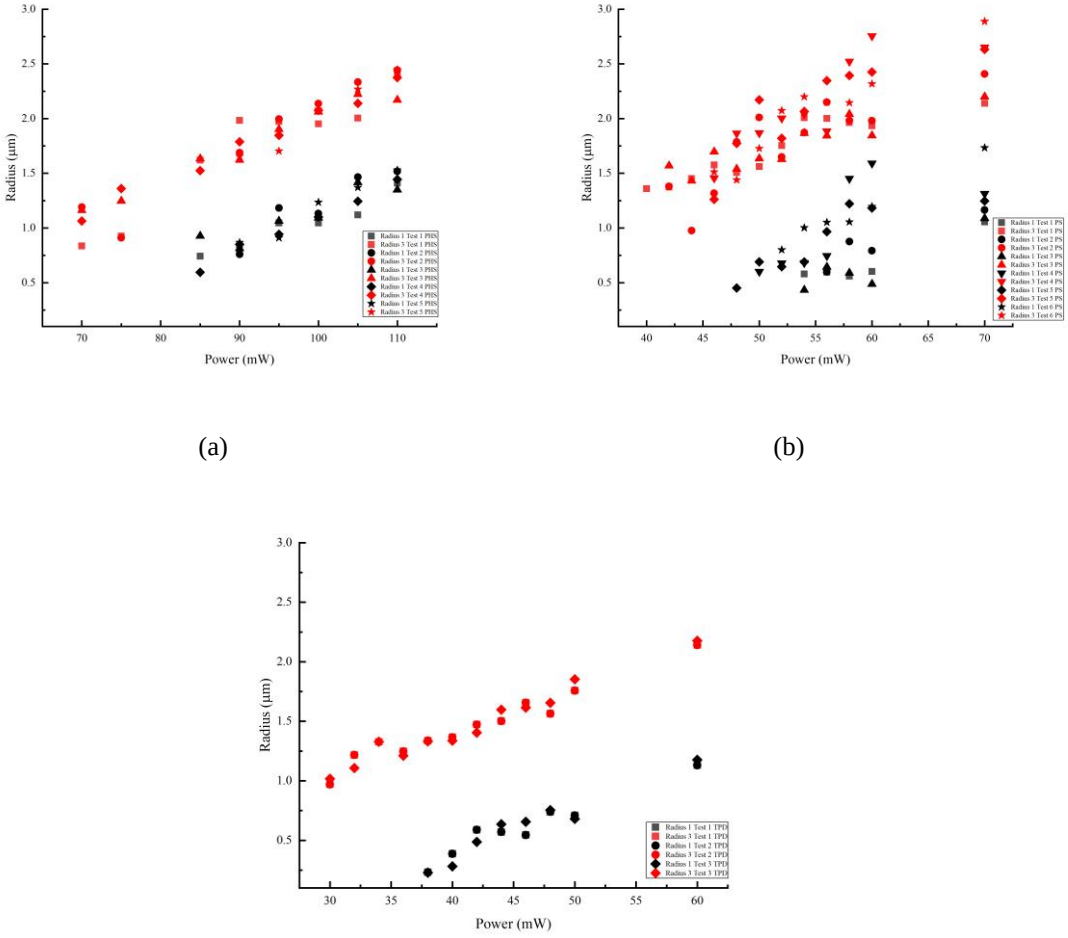

Fig 3.2 Radius versus laser power for (a) PHS, (b) PS and (c) TPD at 1 sec exposure time

From Fig. 3.2, it is observed as expected that radii values – R_1 and R_3 increase linearly with laser power. It is also observed that the power required to dewet PHS film – 70 mW, is much greater than that required for PS film and TPD film which are 40 mW and 30 mW respectively. As mentioned earlier the luminescence of the Mo film is used as an analog

for temperature. Hence the trend between radii values – R_1, R_2, and R_3 and intensity is studied for all the three film materials.

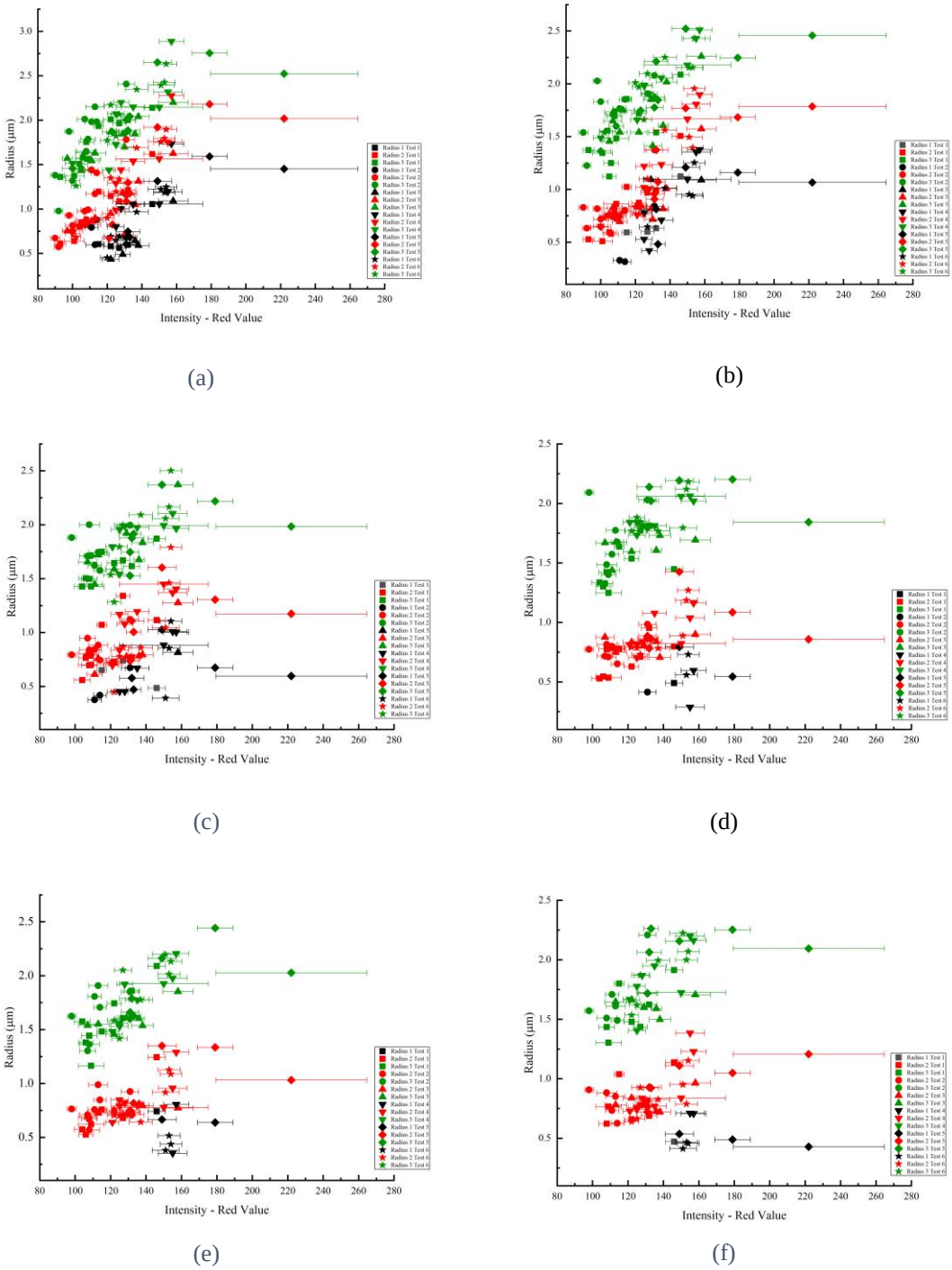

Fig 3.3 Radius versus laser spot intensity at (a) 1 sec, (b) 0.1 sec, (c) 0.01 sec, (d) 0.001 sec, (e) 0.0001 sec and (f) 0.00001 sec exposure time for PS

From Fig. 3.3 the relationship between radii and laser spot intensity can be observed. The plots depict evolution occurring at an earlier time. The plots also suggest that PS dewetting occurs at a high intensity value. The trend when considered after removing the outliers suggests a linear relationship between the radii values and intensity. Having assumed intensity as a measure of local temperature, the trends inherently indicates that above the film T_g, with an increase in local temperature on the film the dewet spot radii will increase. The radii value does not seem to vary drastically over the various exposure times, but is observed that the definition of R_1 is poorly understood at lower exposure times. R_3 as mentioned earlier is the maximum radius of dewetting and this corresponds to the edge of visible dewetting. The advantage with R_3 is that it is the easiest to optically observe, however it is the farthest extent away from the zone of action – the laser spot, making it the coldest extent and therefore there is the possibility of material surface property behavior playing a part during the analysis.

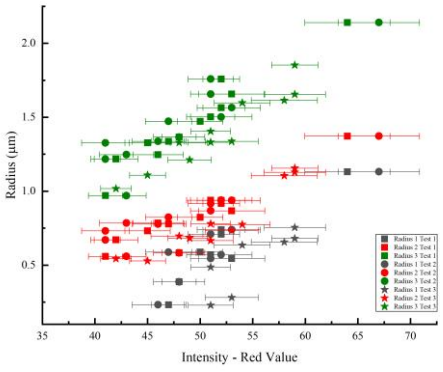

(a)

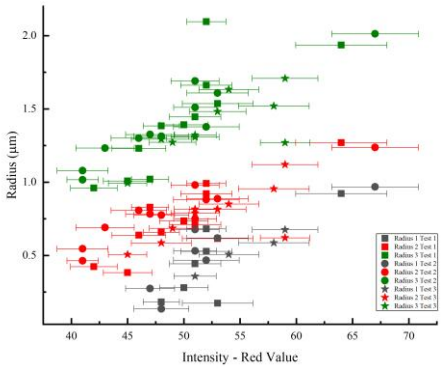

(b)

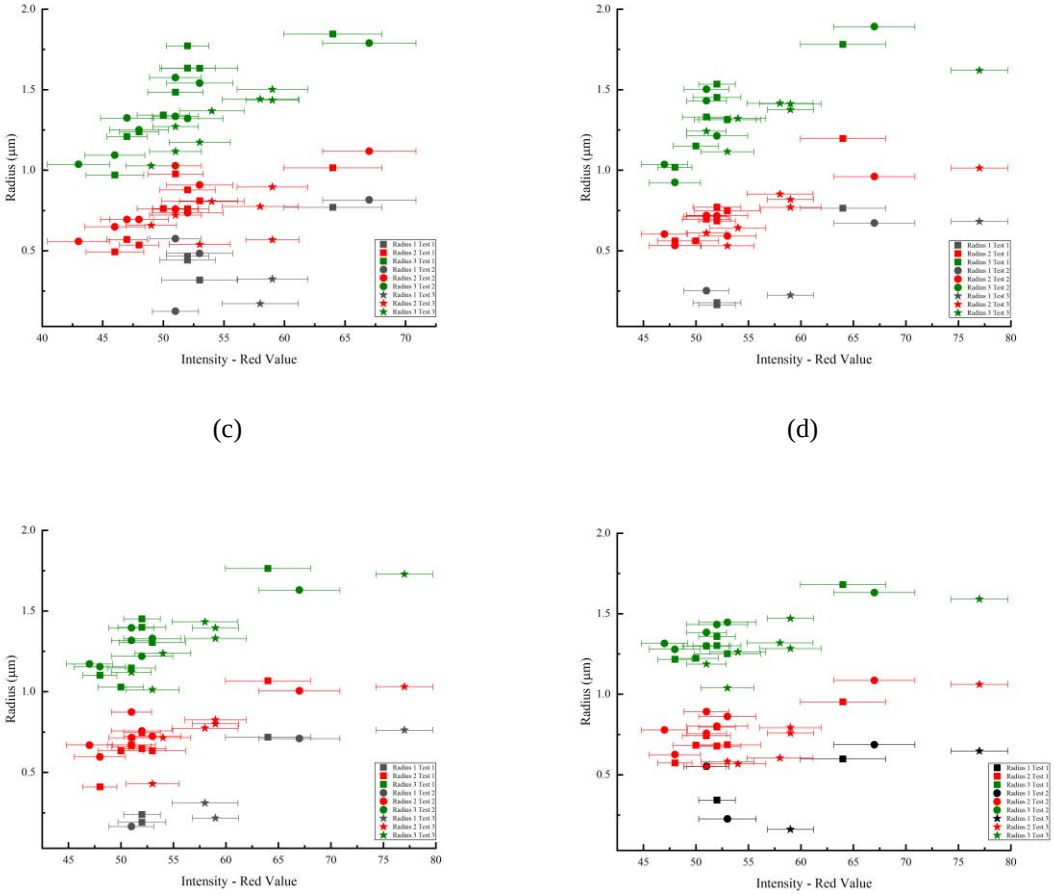

Fig 3.4 Radius versus laser spot intensity at (a) 1 sec, (b) 0.1 sec, (c) 0.01 sec, (d) 0.001 sec, (e) 0.0001 sec and (f) 0.00001 sec exposure time for TPD

From Fig. 3.4 depicts evolution occurring at an earlier time like PS. However, a quick comparison between Fig. 3.3 and Fig. 3.4 depicts that TPD dewetting occurs at much lower intensity value when compared to PS. The trend when considered after removing the outliers once again suggests a linear relationship between the radii values and intensity.

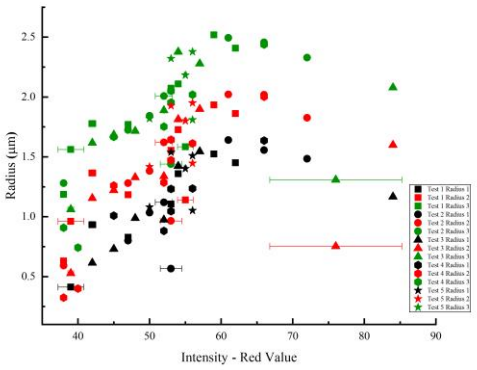

(a)

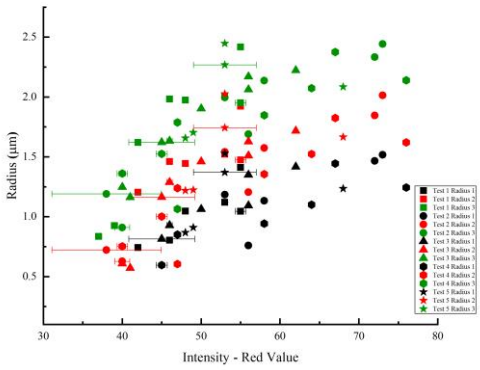

(b)

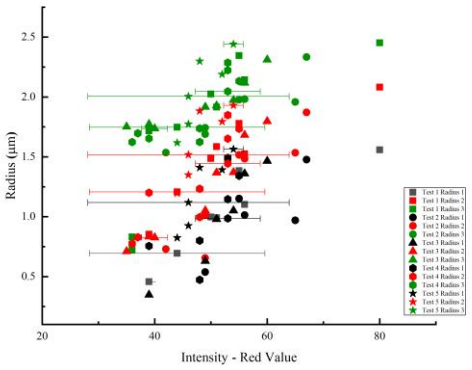

(c)

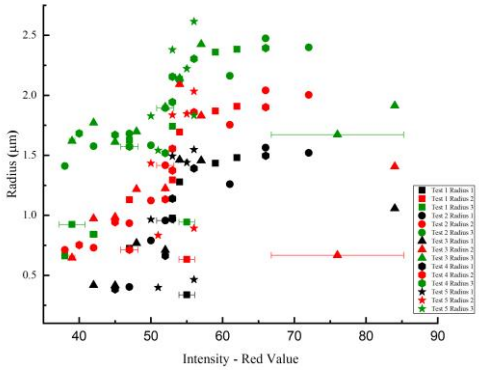

(d)

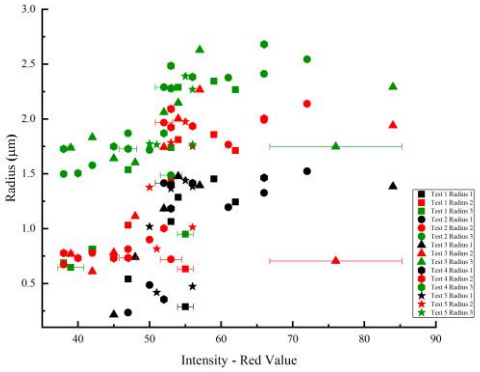

(e)

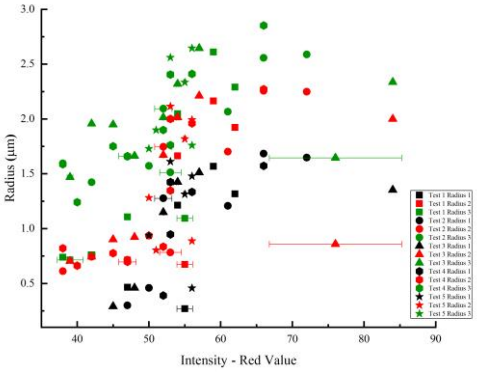

(f)

Fig 3.5 Radius versus laser spot intensity at (a) 10 sec, (b) 1 sec, (c) 0.1 sec, (d) 0.01 sec, (e) 0.001 sec and (f) 0.0001 sec exposure time for PHS

Fig. 3.5 once again depicts evolution occurring at an earlier time for PHS. Comparing Fig. 3.3, Fig. 3.4 and Fig. 3.5 illustrates that PHS dewetting occurs at an intensity value comparable to TPD, but very low when compared to PS. Finally, to visualize material dependency, the radii R_1 and R_3 of all three materials are plotted with respect to intensity. R_2 is disregarded in the current study due to its difficulty in being defined and measured accurately. The comparison is studied at an exposure time of 1 sec at which dewetting has occurred.

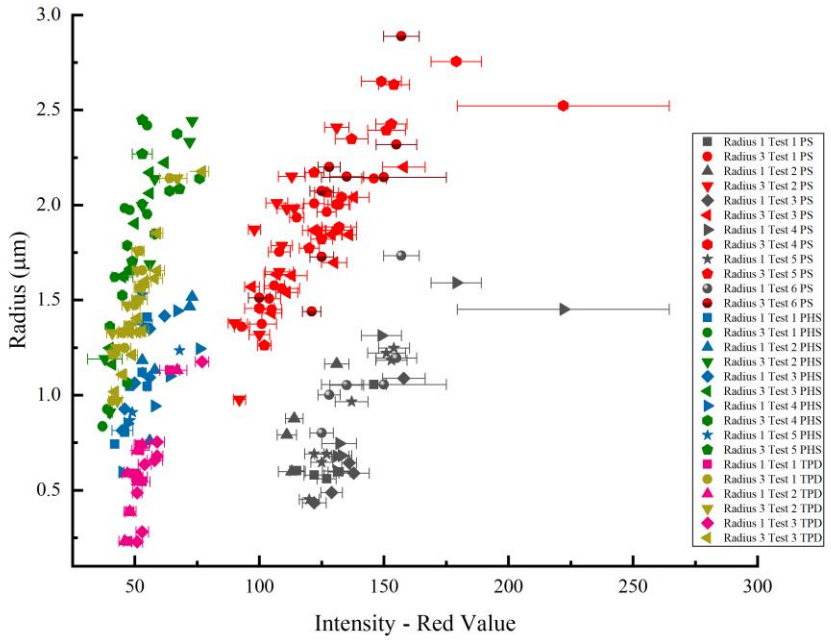

Fig. 3.6 Radius – R_1 and R_3 values versus Intensity for PS, PHS and TPD at 1 sec. exposure time

A few observations can be made from Fig. 3.6. PS dewets at higher intensities while TPD and PHS dewet at much lower intensities. TPD has a small MW when compared to the other two materials. TPD also has the lowest glass transition temperature, $T_g \sim 60$ °C. These two properties can be attributed to the reason behind TPD dewetting at low

intensities. In the case of PS, it has a high MW and high glass transition temperature T_g ~ 100 °C, and this can be used to explain the high intensity required for dewetting. However, PHS shows an eccentric behavior. It dewets at nearly the same intensity at TPD, but possesses a MW comparable to PS and significantly higher than TPD. PHS also possesses a high glass transition temperature T_g ~ 150 °C. This apparent eccentric behavior can be attributed to the hydrophilicity of PHS [10, 70]. Absorbed water on the surface of PHS changes the T_g, which determines the onset of dewetting which is inferred from equation (3). This is explained in further detail in the subsequent section.

3.2 Study of Growth of Radius as a Function of Exposure Time and Intensity

The previous section dealt with extracting values from experiment images and quantifying them in terms of the three radii – R_1, R_2 and R_3. Visualization between radii values and laser spot intensity and the subsequent trends and eccentricities was analyzed for the three different materials. Having quantified and visualized the trends, this section aims at investigating the ability to use the data to potentially obtain information about the material properties.

Focusing on R_1 and R_3, and assuming that there is very small or negligible slip R_0. Fluid mechanics equations help obtain

$$\tau = \beta \nabla T = \beta \frac{dT}{dr} = 2\mu \frac{dv}{dz} \approx \frac{2\mu}{h} \frac{d}{dt}(R_1 - R_0) \approx \frac{2\mu}{h} \frac{dR_1}{dt} \tag{7}$$

The next step in the study was to understand the rate of growth of the radii R_1 and R_3. In order to accomplish this, a semi–log plot was plotted for the three materials. Radii values

– R_1 and R_3 were grouped into different ranges of intensity and then each group was plotted against exposure time.

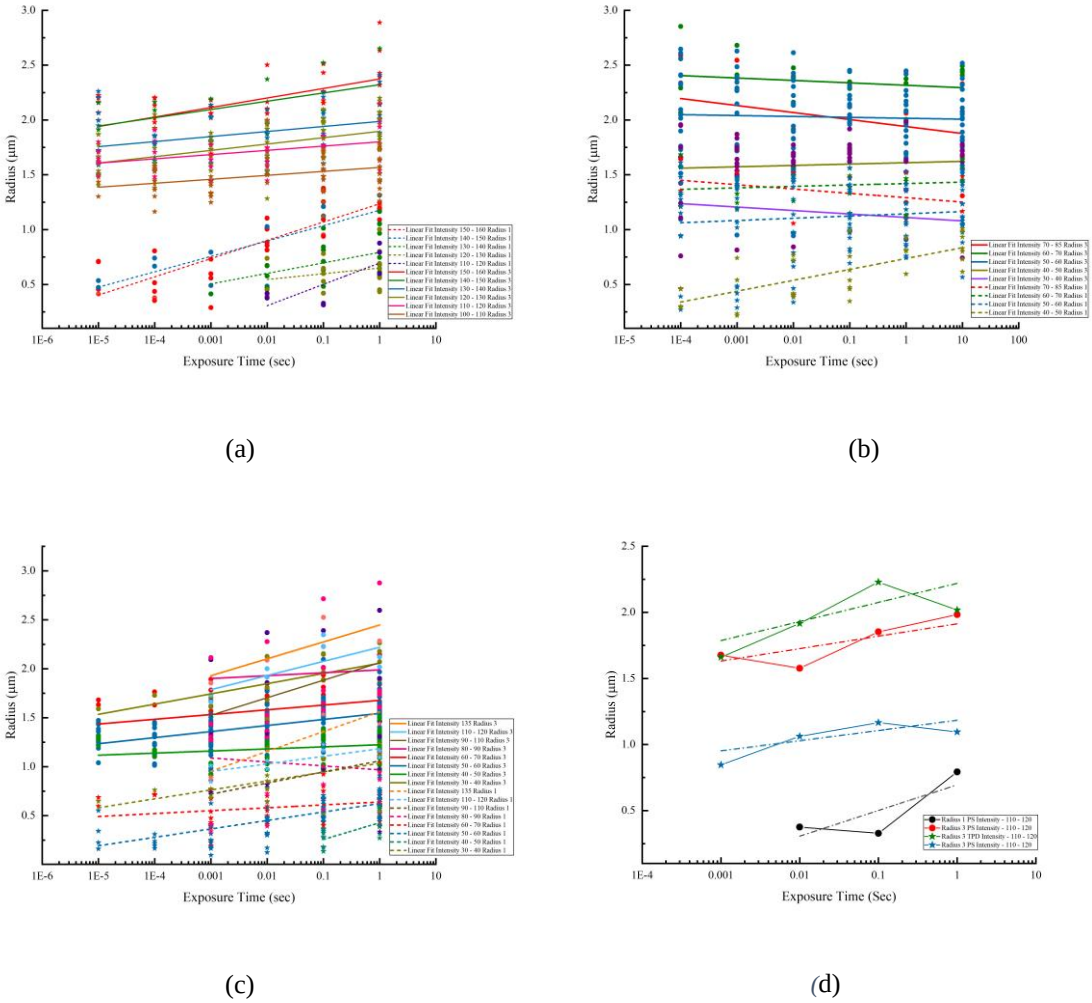

Fig. 3.7 Semi–log plot of growth of radii for various laser spot intensity value ranges for (a) PS, (b) PHS and (c) TPD with linear fit. (d) Semi–log plot of growth of radii for PS and TPD for the same value of laser spot intensity

From Fig. 3.7, it is observed that growth of radii – R_1 and R_3 tend to vary linearly with the logarithm of exposure time. The observed behavior differs from typical dewetting behavior exhibited in studies – the power law [7], though it is possible that we could have fit these

to a power law. The behavior evidenced from Fig. 3.7 would breakdown at exposure time equal to zero, but this is beyond the scope of this study. While the trend line doesn't make physical sense, it fits the data well and as such would be a good starting point. Fig. 3.7 (d) shows that over the same exposure time period and laser spot intensity, growth of radii in the case of TPD is greater when compared to PS, possibly due to lower MW and low T_g. The slope of the linear fit which is equal to the rate of growth of the radii, $\frac{dR}{dt}$ was calculated from Fig. 3.7 (a), (b) and (c) and its variation with intensity was visualized as shown in Fig. 3.8.From Fig. 3.8 it can be observed that for PS and TPD, the rate of change in radius,

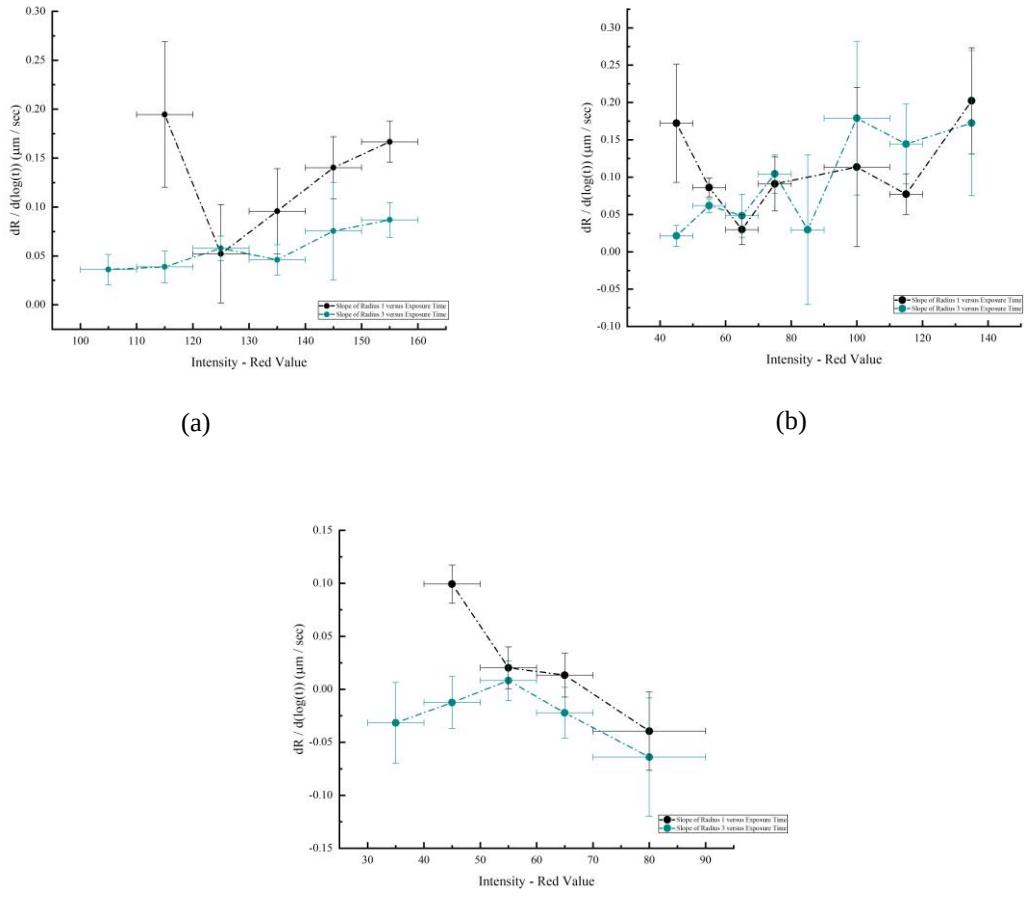

(a) (b)

(c)

Fig. 3.8 Rate of growth of radii versus laser spot intensity value for (a) PS, (b) TPD and (c) PHS

R_1 decreases initially and then starts to increase. It is also observable that for all the three materials $\frac{dR_1}{dt} > \frac{dR_3}{dt}$. Fig. 3.9 compares the rate of change of radii R_1 and R_3 across all materials.

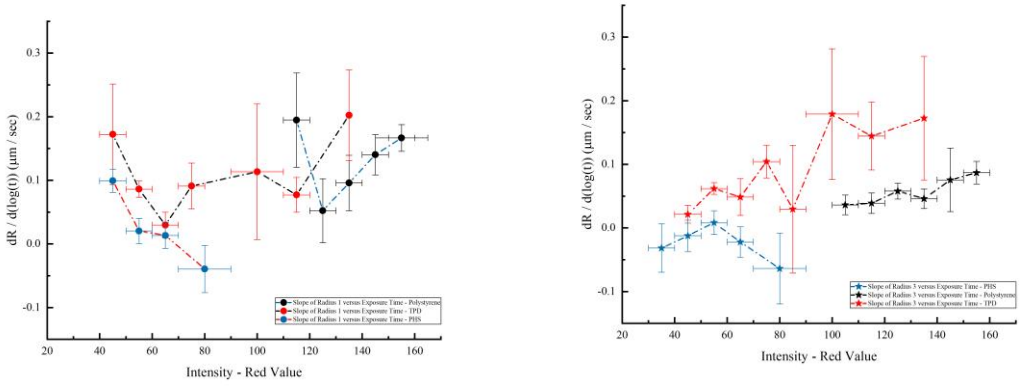

(a) (b)

Fig. 3.9 Rate of growth of radii (a) R_1 and (b) R_3 versus laser spot intensity value for PS, TPD and PHS

The change in radius value is then used to calculate apparent velocity. The apparent velocity is calculated at an exposure time equal to 0.0001 sec.

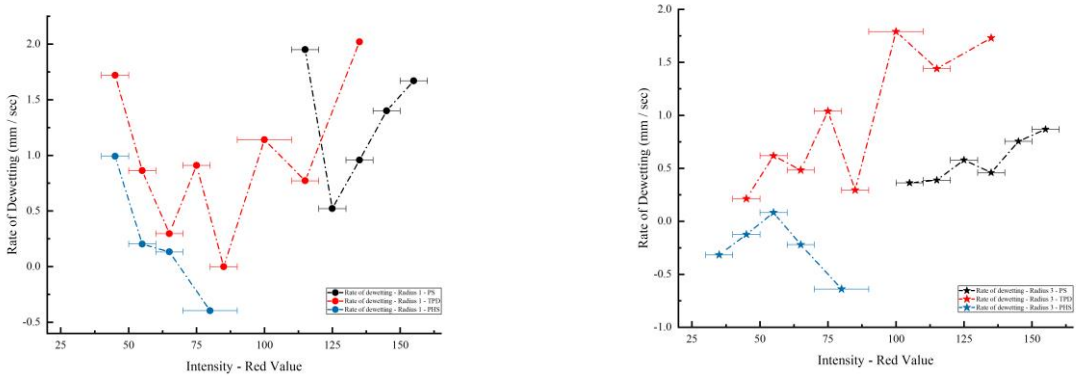

(a) (b)

Fig. 3.10 Rate of dewetting of (a) R_1 (b) R_3 as a function of laser spot intensity

From Fig. 3.9 and 3.10 it can be observed that the dewetting for TPD which has a T_g approximately equal to 60 °C occurs much earlier than dewetting for PS which has a T_g approximately equal to 100 °C. After crossing the apparent T_g, the growth rate of radius – R_1 for both PS and TPD follow a very similar upward trajectory trend. The growth rate of radius for TPD occurs in a broader intensity bandwidth when compared to PS, which occurs in a narrow intensity bandwidth. The rapid change at low intensity is observed in studies that have demonstrated early-stage dewetting having a greater bandwidth [55]. The initial dip in the trend can be attributed to the surface behavior of the thin film, which is the most evident in the case of PHS. If the surface has a higher mobility than the rest of the film, it may rapidly dewet while leaving the rest of the film behind. At higher temperatures, more of the film participates in the dewetting, leading to an apparent reduction of the dewetting speed. PHS merits some additional scrutiny. PHS has a MW close to that of PS and has a high T_g of 150 °C. PHS despite having a much higher T_g, shows a drop or reduction in the growth of dewetting and a very low intensity onset of dewetting.

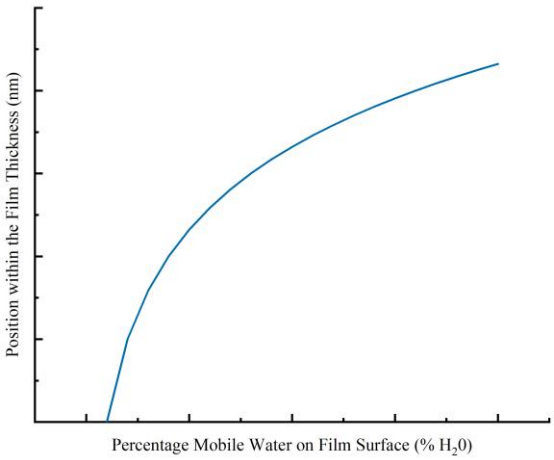

Fig. 3.11 Sketch depicting percentage water content as a function of position within film thickness for PHS

As discussed before, the reason that can be attributed to this is the hydrophilicity of PHS. The dip in the growth rate is not driven by bulk thermocapillary dewetting. This dip arises as a result of watery surface layer on the film which is represented approximately by the plot in Fig. 3.11. Fig. 3.11 approximately depicts the percentage mobile water on the film surface as a function of position within the film thickness. Near the surface of the film the percentage of mobile water is greater when compared to the bulk regions of the film. This means that the effect of the rapid surface dewetting is even greater, as the deeper regions gradually start participating. In addition, the heat will affect the dynamic concentration of water. It is likely that the mobile water-swollen surface layer slows and contracts upon FLaSk annealing due to solvocapillary forces. The local temperatures generated are also strong enough to result in evaporation of this water surface layer resulting in thermal drying. This results in an inward flow. Studies have been conducted that demonstrate this similar effect occurring during dewetting [71-74]. Fig. 3.10 (b) shows that in the case of TPD R_3 grows at a similar rate as R_1. For PS, R_3 growth is slower and less steep when compared to R_1 of PS. In the case of PHS, the R_3 grows at a larger negative rate. However, as mentioned previously R_3 is the radii farthest away from the center of the laser spot and it is also the coldest zone locally. Therefore R_3 represents the region where material properties such as viscoelasticity may have an effect.

CHAPTER 4 – CONCLUSIONS

This study aimed at investigating if FLaSk dewetting would serve as a potential method to probe material properties. In order to achieve this, thin films of Polystyrene (PS), Poly–4–hydroxystyrene (PHS) and N, N′-Bis (3–methylphenyl)–N, N′-diphenylbenzidine (TPD) were spun coat onto a universal heating substrate. These three materials were chosen for their difference in MW and T_g. The film thickness was measured to ensure that all three films lied in the same range and then FLaSk dewetting experiments were performed on the film. The experiments were captured in videos using Thorlabs DCx camera and then the intensity of the laser spot was calculated using a MATLAB program. The dewet pattern and spots were analyzed and captures using Leica Microsystems optical microscope and the radii was analyzed using MATLAB. Intensity and laser power for experiments conducted on the three materials were analyzed using plots and the trend suggested all the materials have the same dewetted profile. Therefore, it was assumed that intensity is an indicator of local temperature. Radii versus intensity plots for all the materials indicated evolution occurring at an earlier time. PS deweted at higher intensities while TPD and PHS deweted at much lower intensities. The low T_g and MW was attributed to the reason behind TPD dewetting at low intensities. In the case of PS, its high MW and high T_g explained the high intensity required for dewetting. The radii value did not seem to vary drastically over the various exposure times, but it was observed that the definition of R_1 was poorly understood at lower exposure times. PHS however showed an eccentric behavior. It deweted at low intensities while possessing a high T_g and MW. This behavior was due to the hydrophilicity of PHS Absorbed water on the surface of PHS changes the T_g, which determined the onset of dewetting. The next step in the study was to understand the rate of

growth of the radii R_1 and R_3. In order to accomplish this, a semi–log plot was plotted for the three materials. It was observed that growth of radii – R_1 and R_3 varied linearly with the logarithm of exposure time and in contrast to the power law behavior in dewetting. The slope of the linear fit which is equal to the rate of growth of the radii and apparent velocity were calculated. The growth rate of radius for TPD occurred in a broader intensity bandwidth when compared to PS, which occurred in a narrow intensity bandwidth. There was an initial dip in the growth rate due to the surface behavior of the thin film, which was very evident in the case of PHS. Once again hydrophilicity of PHS played a major role. The water surface layer slows and contracts upon FLaSk annealing due to solvocapillary forces. The local temperatures generated are also strong enough to result in evaporation of this water surface layer resulting in thermal drying. This resulted in a negative growth or otherwise known as inward flow.

Based on all the above data, the study suggests that these dewetting parameters indicated thermally-dependent behavior. For instance, the slower growth rate for PS and the increased negative rate PHS were consistent with higher viscosity or T_g in (3). The rapid change in growth rate at low intensity were found to be consistent with previously conducted studies that suggest early stage dewetting have a longer range. However, the ability to quantitatively correlate these results to materials properties is currently not possible as the local instantaneous temperature is unknown. Properties such as T_g are extremely sensitive to film thickness and film history, making this a more complex study.

CHAPTER 5 – FUTURE SCOPE OF WORK

Future work would entail discovering further ways to develop a foolproof method to analyze the radii values. Specifically, R_1 and R_2. This would require extensive pixel color gradient and mapping analysis software and the possibility of such a software working in conjunction with the laser setup, where only selected wavelengths are allowed to pass, possess a significant challenge. Setting up a *in situ* high speed camera that could capture pictures and videos of the dewetting process instantaneously and automatically would help accelerate the analysis process. Also, a vast majority of the future work would be to validate the research idea by establishing a standard when it comes to the repeatability of developing thin films whose standard parameters such as thickness are uniform. Validation studies need to be conducted by analyzing polymers whose properties such as MW and T_g are spread over a range, while at the same time well studied. Polystyrene is one of the most well studied polymers and as such conducting FLaSk dewetting experiments with many PS films with varying MW would be a logical next step. Conducting experiments with hydrophilic materials and developing a method to get rid of the water–swollen surface layer and obtaining local instantaneous temperatures while running the experiments are further necessities to improve the study and would propel the next step in realizing the potential of FLaSk dewetting being a method to probe material film properties.

BIBLIOGRAPHY

1. Ioannis Karapanagiotis, W.W.G., D. Fennell Evans, *Dewetting of Thin Polymer Films*. 2000, University of Minnesota.
2. Karki, S., et al., *Thin films as an emerging platform for drug delivery.* Asian Journal of Pharmaceutical Sciences, 2016. **11**(5): p. 559-574.
3. Rokaya, D., et al., *Polymeric materials and films in dentistry: An overview.* Journal of Advanced Research, 2018. **14**: p. 25-34.
4. Kumar, P., et al., *Hybrid porous thin films: Opportunities and challenges for sensing applications.* Biosens Bioelectron, 2018. **104**: p. 120-137.
5. Lee, C.H. *Technology enables soft contact lenses to monitor glucose, medical conditions and deliver medications*. 2018; Available from: https://phys.org/news/2018-06-technology-enables-soft-contact-lenses.html.
6. Wnek, G., *Polymers*, in *Encyclopedia of Biomaterials and Biomedical Engineering, Second Edition - Four Volume Set*. 2008. p. 2275-2281.
7. Reiter, G., *Probing Properties of Polymers in Thin Films Via Dewetting*, in *Glass Transition, Dynamics and Heterogeneity of Polymer Thin Films*. 2012. p. 29-63.
8. Sharma, S., et al., *Dewetting properties of polystyrene homopolymer thin films on grafted polystyrene brush surfaces.* High Performance Polymers, 2000. **12**(4): p. 581-586.
9. Tsui, O.K.C., T.P. Russell, and C.J. Hawker, *Effect of Interfacial Interactions on the Glass Transition of Polymer Thin Films.* Macromolecules, 2001. **34**(16): p. 5535-5539.
10. Tate, R.S., et al., *Extraordinary elevation of the glass transition temperature of thin polymer films grafted to silicon oxide substrates.* The Journal of Chemical Physics, 2001. **115**(21): p. 9982-9990.
11. *Understanding the Rheological Characteristics of Thermoplastic Polymers*. 2015; Available from: https://www.azom.com/article.aspx?ArticleID=12100.
12. Chen, D.T.N., et al., *Rheology of Soft Materials.* Annual Review of Condensed Matter Physics, 2010. **1**(1): p. 301-322.
13. Mitsoulis, E., *The Effect of Rheology in Polymer Processing: A Simulation Point of View*. 2018.
14. Hyeran Kang, Q.W., Paul A. Janmey, Jay X. Tang, Enrico Conti, Fred C. MacKintosh, *Nonlinear Elasticity of Stiff Filament Networks: Strain Stiffening, Negative Normal Stress, and Filament Alignment in Fibrin Gels.* Journal of Physical Chemistry B, 2009: p. 3799–3805.
15. Cornelis Storm, J.J.P., F. C. MacKintosh, T. C. Lubensky, Paul A. Janmey, *Nonlinear elasticity in biological gels.* Nature, 2005. **435**.
16. Gardel, M.L., et al., *Stress-dependent elasticity of composite actin networks as a model for cell behavior*. Phys Rev Lett, 2006. **96**(8): p. 088102.
17. Kasza, K.E., et al., *Nonlinear elasticity of stiff biopolymers connected by flexible linkers.* Phys Rev E Stat Nonlin Soft Matter Phys, 2009. **79**(4 Pt 1): p. 041928.

18. Ewoldt, R.H., A.E. Hosoi, and G.H. McKinley, *New measures for characterizing nonlinear viscoelasticity in large amplitude oscillatory shear.* Journal of Rheology, 2008. **52**(6): p. 1427-1458.
19. Olmsted, P.D., *Perspectives on shear banding in complex fluids.* Rheologica Acta, 2008. **47**(3): p. 283-300.
20. Boukany, P.E. and S.-Q. Wang, *Nature of steady flow in entangled fluids revealed by superimposed small amplitude oscillatory shear.* Journal of Rheology, 2009. **53**(6): p. 1425-1435.
21. Coussot, P., et al., *Coexistence of liquid and solid phases in flowing soft-glassy materials.* Phys Rev Lett, 2002. **88**(21): p. 218301.
22. T.G. Mason, H.G., D.A. Weitz, *Rheology of complex fluids measured by dynamic light scattering.* Journal of Molecular Structure, 1996. **383**: p. 81-90.
23. Michael J. Solomon, A.S.A., Kurt F. Seefeldt, Anongnat Somwangthanaroj, Priya Varadan, *Rheology of Polypropylene/Clay Hybrid Materials.* Macromolecules (USA), 2001. **34**: p. 1864 - 1872.
24. Zhaohui Yang, Y.F., Fuk Kay Lee, Chi-Hang Lam, Ophelia K. C.Tsui, *Glass Transition Dynamics and Surface Layer Mobility in Unentangled Polystyrene Films.* Science, 2010. **328**: p. 1676(4).
25. J. A. Forrest, K.D.-V., J. R. Stevens, J. R. Dutcher, *Effect of Free Surfaces on the Glass Transition Temperature of Thin Polymer Films.* Physical Review Letters, 1996. **77**: p. 2002 - 2005.
26. McGraw, J.D., N.M. Jago, and K. Dalnoki-Veress, *Capillary levelling as a probe of thin film polymer rheology.* Soft Matter, 2011. **7**(17).
27. Christopher M. Evans, H.D., Wolter F. Jager, John M. Torkelson, *Fragility is a Key Parameter in Determining the Magnitude of Tg-Confinement Effects in Polymer Films.* Macromolecules (USA), 2013. **46**(15): p. 6091 - 6103.
28. Zuo, B., et al., *Probing the rheological properties of supported thin polystyrene films by investigating the growth dynamics of wetting ridges.* Soft Matter, 2016. **12**(28): p. 6120-31.
29. A.A. Svintsov, O.V.T., S.I. Zaitsev, *Thin NIL films viscosity and rheological nano-probe.* 2007 Digest of papers Microprocesses and Nanotechnology, 2007: p. 284-285.
30. P.M. McGuiggana, D.J.Y., *Measurement of the loss tangent of a thin polymeric film using the atomic force microscope.* Journal of Materials Research, 2004. **19**: p. 387 - 395.
31. Daley, C.R., et al., *Comparing surface and bulk flow of a molecular glass former.* Soft Matter, 2012. **8**(7): p. 2206-2212.
32. Glor, E.C., G.V. Angrand, and Z. Fakhraai, *Exploring the broadening and the existence of two glass transitions due to competing interfacial effects in thin, supported polymer films.* The Journal of Chemical Physics, 2017. **146**(20): p. 203330.
33. Glor, E.C., R.J. Composto, and Z. Fakhraai, *Glass Transition Dynamics and Fragility of Ultrathin Miscible Polymer Blend Films.* Macromolecules, 2015. **48**(18): p. 6682-6689.
34. Zhang, Y. and Z. Fakhraai, *Invariant Fast Diffusion on the Surfaces of Ultrastable and Aged Molecular Glasses.* Physical Review Letters, 2017. **118**(6): p. 066101.

35. Zhang, Y., et al., *Long-range correlated dynamics in ultra-thin molecular glass films.* The Journal of Chemical Physics, 2016. **145**(11): p. 114502.
36. Zhang, Y. and Z. Fakhraai, *Decoupling of surface diffusion and relaxation dynamics of molecular glasses.* Proceedings of the National Academy of Sciences, 2017.
37. Konstantin G. Kornev, Y.G., Pavel Aprelev, Alexander Tokarev, *Magnetic rotational spectroscopy for probing rheology of nanoliter droplets and thin films.*
38. Reiter, G., *Dewetting of thin polymer films.* Phys Rev Lett, 1992. **68**(1): p. 75-78.
39. Gabriele, S., et al., *Viscoelastic dewetting of constrained polymer thin films.* Journal of Polymer Science Part B: Polymer Physics, 2006. **44**(20): p. 3022-3030.
40. Saulnier, F., E. Raphael, and P.G. De Gennes, *Dewetting of thin polymer films near the glass transition.* Phys Rev Lett, 2002. **88**(19): p. 196101.
41. Dalnoki-Veress K, N.B.G., Roth C, Dutcher J.R., *Hole formation and growth in freely standing polystyrene films.* Phys. Rev. E, 1999. **59**(2): p. 2153-2156.
42. Masson, J.L. and P.F. Green, *Viscosity of entangled polystyrene thin film melts: Film thickness dependence.* Phys Rev E Stat Nonlin Soft Matter Phys, 2002. **65**(3 Pt 1): p. 031806.
43. Wang, H., et al., *Dramatic Increase in Polymer Glass Transition Temperature under Extreme Nanoconfinement in Weakly Interacting Nanoparticle Films.* ACS Nano, 2018. **12**(6): p. 5580-5587.
44. Hor, J.L., et al., *Effect of Polymer-Nanoparticle Interactions on the Viscosity of Unentangled Polymers under Extreme Nanoconfinement during Capillary Rise Infiltration.* Soft Matter, 2018.
45. Ilton, M., et al., *Adsorption-induced slip inhibition for polymer melts on ideal substrates.* Nature Communications, 2018. **9**(1): p. 1172.
46. Chai, Y., et al., *A Direct Quantitative Measure of Surface Mobility in a Glassy Polymer.* Science, 2014. **343**(6174): p. 994-999.
47. McGraw, J.D., et al., *Capillary leveling of stepped films with inhomogeneous molecular mobility.* Soft Matter, 2013. **9**(34): p. 8297-8305.
48. McGraw, J.D., et al., *Self-Similarity and Energy Dissipation in Stepped Polymer Films.* Physical Review Letters, 2012. **109**(12): p. 128303.
49. Xue, L. and Y. Han, *Pattern formation by dewetting of polymer thin film.* Progress in Polymer Science, 2011. **36**(2): p. 269-293.
50. Telford, A.M., S.C. Thickett, and C. Neto, *Functional patterned coatings by thin polymer film dewetting.* J Colloid Interface Sci, 2017. **507**: p. 453-469.
51. Marangoni, C., *Difesa della teoria dell'elasticità superficiale dei liquidi. Plasticità superficiale.* Il Nuovo Cimento (1869-1876), 1870. **3**(1): p. 97-115.
52. Caspers, P., Lucassen, G., & Puppels, G., *Combined In Vivo Confocal Raman Spectroscopy and Confocal Microscopy of Human Skin.* Biophysical Journal, 2003. **85**(1): p. 572-580.
53. Singer, J.P., *Thermocapillary approaches to the deliberate patterning of polymers.* Journal of Polymer Science Part B: Polymer Physics, 2017. **55**(22): p. 1649-1668.
54. Singer, J.P., et al., *Alignment and reordering of a block copolymer by solvent-enhanced thermal laser direct write.* Polymer, 2014. **55**(7): p. 1875-1882.

55. Singer, J.P., S.E. Kooi, and E.L. Thomas, *Focused laser-induced marangoni dewetting for patterning polymer thin films.* Journal of Polymer Science Part B: Polymer Physics, 2016. **54**(2): p. 225-236.
56. Singer, J.P., et al., *Direct-Write Thermocapillary Dewetting of Polymer Thin Films by a Laser-Induced Thermal Gradient.* Advanced Materials, 2013. **25**(42): p. 6100-6105.
57. Elashnikov, R., et al., *Patterning of ultrathin polymethylmethacrylate films by in-situ photodirecting of the Marangoni flow.* Applied Surface Science, 2017. **394**: p. 562-568.
58. Elashnikov, R., et al., *Laser patterning of transparent polymers assisted by plasmon excitation.* Soft matter, 2018.
59. Ilton, M., C. DiMaria, and K. Dalnoki-Veress, *Direct measurement of the critical pore size in a model membrane.* Physical Review Letters, 2016. **117**(25): p. 257801.
60. Elashnikov, R., et al., *Patterning of ultrathin polymethylmethacrylate films by in-situ photodirecting of the Marangoni flow.* Applied Surface Science, 2016.
61. Bordeenithikasem, P., et al., *Determination of critical cooling rates in metallic glass forming alloy libraries through laser spike annealing.* Sci Rep, 2017. **7**(1): p. 7155.
62. DeMaggio, G., et al., *Interface and surface effects on the glass transition in thin polystyrene films.* Physical Review Letters, 1997. **78**(8): p. 1524.
63. Roth, C.B., et al., *Eliminating the enhanced mobility at the free surface of polystyrene: fluorescence studies of the glass transition temperature in thin bilayer films of immiscible polymers.* Macromolecules, 2007. **40**(7): p. 2568-2574.
64. Savin Daniel, A., et al., *Synthesis and characterization of silica-graft-polystyrene hybrid nanoparticles: Effect of constraint on the glass-transition temperature of spherical polymer brushes.* Journal of Polymer Science Part B: Polymer Physics, 2002. **40**(23): p. 2667-2676.
65. Yang, Z., et al., *Glass transition dynamics and surface layer mobility in unentangled polystyrene films.* Science, 2010. **328**(5986): p. 1676-1679.
66. Mooradian, A., *Photoluminescence of Metals.* Physical Review Letters, 1969. **22**(5): p. 185-187.
67. Apell, P., R. Monreal, and S. Lundqvist, *Photoluminescence of noble metals.* Physica Scripta, 1988. **38**(2): p. 174.
68. Suezawa, M., Sasaki, Y., & Sumino, K, *Dependence of Photoluminescence on Temperature in Dislocated Silicon Crystals.* physica status solidi (a), 1983. **79**(1): p. 173 - 181.
69. Williams, M.L., R.F. Landel, and J.D. Ferry, *The temperature dependence of relaxation mechanisms in amorphous polymers and other glass-forming liquids.* Journal of the American Chemical society, 1955. **77**(14): p. 3701-3707.
70. Augsburg, A., et al., *Determination of contact angles and solid surface tensions of poly(4-X-styrene) films.* Acta Polymerica, 1999. **49**(8): p. 417-426.
71. Atena, A., & Khenner, M. , *Thermocapillary effects in driven dewetting and self-assembly of pulsed laser-irradiated metallic films.* 2009.
72. McGraw, J., Chan, T., Maurer, S., Salez, T., Benzaquen, M., Raphael, E., Brinkmann, M, Jacobs, K, *Slip-mediated dewetting of polymer microdroplets.*

Proceedings of the National Academy of Sciences of the United States, 2016. **113**(5).

73. Afkhami, S., & Kondic, L. , *On the dewetting of liquefied metal nanostructures.* Journal of Engineering Mathematics, 2015. **94**(1): p. 5-18.
74. Poulard, C., & Damman, P., *Control of spreading and drying of a polymer solution from marangoni flows.* EPL (Europhysics Letters), 2007. **80**(6): p. 5.